Triton binding energy and neutron-deuteron scattering up to next-to-leading order in chiral effective field theory

Young-Ho Song,[1,*] Rimantas Lazauskas,[2,†] and U. van Kolck[3,4,‡]
[1]*Rare Isotope Science Project, Institute for Basic Science, Daejeon 305-811, Korea*
[2]*Université de Strasbourg, CNRS IPHC UMR 7178, F-67000 Strasbourg, France*
[3]*Institut de Physique Nucléaire, CNRS/IN2P3, Université Paris-Sud, Université Paris-Saclay, F-91406 Orsay Cedex, France*
[4]*Department of Physics, University of Arizona, Tucson, Arizona 85721, USA*
(Received 30 December 2016; revised manuscript received 14 June 2017; published 2 August 2017)

Determination of the proper power-counting scheme is an important issue for the systematic application of Chiral Effective Field Theory in nuclear physics. We analyze the cutoff dependence of three-nucleon observables (the neutron-deuteron scattering lengths and the triton binding energy) at the leading and next-to-leading orders of a power counting that ensures order-by-order renormalization in the two-nucleon system. Our results confirm that, as usually assumed in the literature, three-body forces are not needed for renormalization of the three-nucleon system up to next-to-leading order.

DOI: 10.1103/PhysRevC.96.024002

I. INTRODUCTION

Hadronic effective field theories (EFTs) provide a representation of QCD at the relatively large distances involved in nuclear dynamics. Chiral EFT, which includes nucleons, pions, and the lightest baryon excited states as active degrees of freedom, aims at an expansion of nuclear amplitudes in powers of $Q/M_{\rm QCD}$, where the typical external momentum is of the order of the pion mass, $Q \sim m_\pi$, and $M_{\rm QCD} \sim 1$ GeV is the characteristic scale of QCD.

The investigation of nuclear forces and currents in Chiral EFT was initiated in the early 1990s [1–8], based on a two-step scheme proposed by Weinberg. The first step is to calculate the nuclear potential and currents—the sum of "irreducible" diagrams—up to a given order, that is, a given power of $Q/M_{\rm QCD}$. The contributions of each order are given by the usual power counting of Chiral Perturbation Theory (ChPT), assuming that short-range nuclear interactions obey the same naive dimensional analysis (NDA) [9] used in the purely perturbative problems involving at most one nucleon. The second step is to solve the Schrödinger or Lippmann-Schwinger (LS) equations exactly with the potential truncated at the desired order, which corresponds to the nonperturbative iteration of the potential subdiagrams. Following the initial successes in explaining some of the qualitative features of models [2–8], the application of ChPT to nuclear forces and currents has reached the point where a very accurate description of data can be achieved—see, for example, Refs. [10–12] and references therein.

Renormalization-group invariance (RGI) is the crucial ingredient that separates nuclear EFTs from the phenomenological models that preceded them. RGI guarantees control over arbitrary choices made during the regularization procedure, such as the functional form of the regulator and the numerical value of the regulator parameter(s). Although initial numerical results using Gaussian regulators with a cutoff in the range $\Lambda = 500 \to 1000$ MeV seemed to indicate only moderate cutoff dependence [8], examples have accumulated since the mid-1990s showing that Weinberg's scheme is not consistent with RGI in the two-nucleon sector.

In the spin-singlet S wave ($^1S_0$), NDA prescribes a single chiral-invariant counterterm at leading order (LO) together with one-pion exchange (OPE), but RGI demands also a chiral-breaking counterterm [13,14], which according to NDA would appear only at relative $\mathcal{O}(Q^2/M_{\rm QCD}^2)$, or next-to-next-to-leading order (N^{2}LO).[1] Contrary to the LO chiral-invariant counterterm, this chiral-breaking interaction involves pions. Its enhancement over NDA affects processes with external pions but has only mild effects on the two-nucleon amplitude at a fixed pion mass. However, other two-nucleon channels suffer from larger cutoff effects stemming from the singular nature of the OPE tensor force. In each spin-triplet channel, where the OPE tensor force is attractive, the solution of the LS equation generates bound states that cross threshold as the cutoff Λ increases beyond about 1 GeV [15,16]. In Weinberg's scheme OPE is iterated in all waves, but NDA prescribes an LO counterterm only in the $^3S_1$ wave. NDA erroneously assigns counterterms in the attractive P, D,... waves to N^{2}LO, N^{4}LO,..., respectively. At higher orders in Weinberg's scheme, cutoff dependence does not disappear [17–21].

One way to achieve RGI is to relegate pion exchange to higher orders, which are treated in perturbation theory at the amplitude level [22,23]. Unfortunately, in the spin-triplet partial waves where OPE is attractive, pions do not seem perturbative for momenta $Q \gtrsim 100$ MeV [24]. Indeed, a

*yhsong@ibs.re.kr
†rimantas.lazauskas@iphc.cnrs.fr
‡vankolck@ipno.in2p3.fr

[1]Note that in part of the literature [11,12] this order is denoted as next-to-leading order (NLO) because *under the assumption of NDA* parity and time reversal ensure that $\mathcal{O}(Q/M_{\rm QCD})$ contributions vanish. We prefer to denote $\mathcal{O}(Q^n/M_{\rm QCD}^n)$ corrections as N^{n}LO to accommodate the known violation of NDA.

careful argument [25] indicates that pions are nonperturbative within the EFT regime in the ${}^3S_1$-${}^3D_1$, ${}^3P_0$, ${}^3P_2$-${}^3F_2$, and possibly ${}^3D_2$ and ${}^3D_3$-${}^3G_3$ waves. Thus, one should iterate OPE only in the waves where iteration is needed, together with a chiral-invariant counterterm in each of these waves [15]. RGI, as well as a reasonable description of data, can be maintained at higher orders as long as these corrections are treated at the amplitude level in distorted-wave perturbation theory [26–30], as advocated in Refs. [14,15,31,32].

Given the failure of NDA in the two-nucleon sector of Chiral EFT, it is important to ascertain if few-body forces are not enhanced, as is the case for Pionless EFT [33–35]. Under the assumption of NDA, three-body forces appear only at subleading orders, and more-body forces at even higher orders [3–5,7]. Virtually every application of ChPT in nuclear physics [10–12] has assumed this to be appropriate.

Here we use RGI as a diagnostic tool for the appearance of three-nucleon forces. A preliminary study of this question was made in Ref. [15], where the triton binding energy was shown to approach a constant for cutoff values up to 4 GeV with a separable momentum regulator of the form $f_4(p/\Lambda) = \exp[-p^4/\Lambda^4]$, after the two-nucleon problem was properly renormalized. We extend the LO cutoff dependence analysis of Nogga *et al.* [15] significantly. For the same regulator function, we extend the two-nucleon renormalization to cutoff values as high as 10 GeV. We also examine the effects of a change in regulator function to $f_2(p/\Lambda) = \exp[-p^2/\Lambda^2]$ and $f_6(p/\Lambda) = \exp[-p^6/\Lambda^6]$. Our results for the triton binding energy are consistent with those of Nogga *et al.* and we find similar cutoff dependence for the quartet and doublet neutron-deuteron scattering lengths. An analysis of the residual cutoff dependence of two- and three-nucleon observables confirms that RGI does not require an LO three-body force but does indicate the appearance of an NLO correction in the ${}^1S_0$ channel, as pointed out by Long and Yang [30]. Then, we extend our analysis to include this NLO correction. Again we find convergence of three-nucleon observables with increasing cutoff, which suggests that the three-body force is at least N^{2}LO. However, there is some indirect evidence that this three-body force might be numerically significant.

Of course we can only calculate a limited set of three-nucleon observables[2] and cannot exclude the possibility that other observables show relevant cutoff dependence. However, being sensitive to many interactions, the observables we study are likely to be a good diagnostic of incomplete renormalization. Very recently, Kievsky *et al.* [36] have argued that for consistency with Pionless EFT a three-nucleon force should be included at LO in Chiral EFT as well. Although a higher order interaction can always be promoted in order to improve agreement with data, we find no renormalization rationale for promotion of the three-nucleon force in Chiral EFT, as in Pionless EFT [33–35].

This paper is organized as follows. In Sec. II, the RGI formulation of Chiral EFT at LO and NLO is presented, together with the details of our calculation. Our numerical results are shown in Sec. III, and Sec. IV offers a summary and conclusions.

[2]From here on, unless noted otherwise, by "three-nucleon observables" we mean the triton binding energy and the quartet and doublet neutron-deuteron scattering lengths.

II. THEORETICAL FRAMEWORK

An EFT is based on the most general Lagrangian (or Hamiltonian) built from the relevant low-energy degrees of freedom, which is constrained only by some assumed symmetries. Here we are interested in typical momenta $Q \sim m_\pi$, so we consider nucleons and pions (the lightest nucleon excitations contributing only beyond NLO) under the QCD symmetries, including an $\mathrm{SU}(2)_L \times \mathrm{SU}(2)_R$ chiral symmetry explicitly broken by the quark masses.

The basic assumption of EFT is that dynamics at a low-energy scale does not depend on detailed assumptions about the short-range dynamics, which is encrypted in the interaction strengths, or low-energy constants (LECs). The LECs depend on the regularization parameter Λ so that observables, obtained from scattering amplitudes, are insensitive to the arbitrary regularization function. Here we denote the breakdown scale of the current version of Chiral EFT as $M_{\rm hi} \lesssim M_{\rm QCD}$, and we will be concerned with the LECs that encode short-range two- and three-nucleon interactions.

Because the EFT includes an infinite number of interactions, it is imperative to organize them according to their importance to amplitudes. We estimate the importance of contributions according to the power of $Q/M_{\rm hi}$ and refer to the relation between this power and the interactions in the Lagrangian as power counting. Power counting offers a rationale to truncate the expansion of observables with a relative error $(Q/M_{\rm hi})^n$, where $n \geqslant 1$ is the power of the next corrections. We use some observables to fix the dependence of the LECs on Λ; these observables remain exactly cutoff independent. The residual cutoff dependence of other observables will be considered small as long as it is of the form $(Q/\Lambda)^n$. In this case, variation for the cutoff from $M_{\rm hi}$ to a much larger value gives an estimate of the overall systematic error of the truncation.

A. Leading order

In the original power counting scheme of Weinberg [1], the LO potential includes OPE between two nucleons. Denoting the spin (isospin) of nucleon i by $\boldsymbol{\sigma}_i/2$ ($\vec{\tau}_i/2$) and the momentum transfer by $\boldsymbol{q} = \boldsymbol{p}' - \boldsymbol{p}$, where $\boldsymbol{p}$ ($\boldsymbol{p}'$) is the initial (final) relative momentum, the expression of OPE potential in momentum space is written as

$$V_{1\pi}^{(0)}(\boldsymbol{p}', \boldsymbol{p}) = -\frac{1}{(2\pi)^3}\frac{g_A^2}{4f_\pi^2}\vec{\tau}_1 \cdot \vec{\tau}_2 \frac{\boldsymbol{\sigma}_1 \cdot \boldsymbol{q}\, \boldsymbol{\sigma}_2 \cdot \boldsymbol{q}}{\boldsymbol{q}^2 + m_\pi^2}, \qquad (1)$$

where $g_A = 1.29$ is the pion-nucleon axial coupling, $f_\pi = 92.4$ MeV is the pion decay constant, and $m_\pi = 138$ MeV is the pion mass. This potential has central and tensor components.

NDA suggests that at the same order one should supplement the ${}^1S_0$ and ${}^3S_1$ partial waves with contact interactions. In contrast, the analysis of Ref. [15] shows that RGI requires the presence of contact interactions at LO in *all* waves

where the singular pion tensor force is attractive and treated nonperturbatively. Still, as the centrifugal barrier increases, the low-energy effects of the tensor force diminish, and for large angular momentum l OPE does not need to be iterated within the regime of validity of the EFT. Only now is it being investigated how the l suppression compares with the $Q/M_{\rm hi}$ expansion, and so far results are limited to spin-singlet channels [37]. Since neither the l suppression nor the value of $M_{\rm hi}$ are known precisely, one is not able to make a sharp separation between waves where OPE is nonperturbative or perturbative.

In this work we consider an LO contact potential

$$V_{\rm ct}^{(0)}(\boldsymbol{p}',\boldsymbol{p}) = \frac{1}{(2\pi)^3}\big[\tilde{C}_{^1S_0}P_{^1S_0} + \tilde{C}_{^3S_1}P_{^3S_1} + C_{^3P_0}\,p'p\,P_{^3P_0} + C_{^3P_2}\,p'p\,P_{^3P_2} + C_{^3D_2}\,p'^2p^2\,P_{^3D_2} + C_{^3D_3}\,p'^2p^2\,P_{^3D_3}\big], \quad (2)$$

where $C_X = C_X(\Lambda)$ and P_X are, respectively, a LEC in and the projector onto partial wave X. Several comments are in order:

(1) OPE has a chiral-invariant δ-function singularity in coordinate space that contributes in both $^1S_0$ and $^3S_1$ waves. NDA prescribes chiral-symmetric contact interactions in these waves at LO, and we absorb the OPE δ function in the corresponding LECs. The remaining part of OPE in $^1S_0$ (a Yukawa function) is not singular in itself, but together with the chiral-symmetric contact interaction produces an $m_\pi^2 \ln\Lambda$ divergence, which requires at least one chiral-breaking counterterm [13,14]. Although this interaction has a different form than the chiral-symmetric contact interaction, since it involves additional pion fields, it does not produce new effects up to NLO in the processes of interest here, *as long as the pion mass is fixed*. In Eq. (2) we denote by $\tilde{C}_{^1S_0}$, $\tilde{C}_{^3S_1}$ the original chiral-invariant LECs together with the OPE δ-function coefficient and (in $^1S_0$) the chiral-breaking LEC.

(2) Numerical experimentation [15] and a semianalytical argument [25] suggest that OPE is nonperturbative in all P waves. OPE is not singular in $^1P_1$ and the tensor force is repulsive in $^3P_1$. Thus, of the P waves, only $^3P_0$ and $^3P_2$ require counterterms $C_{^3P_0}$ and $C_{^3P_2}$, respectively, at LO—although from NDA they would be expected only at N^{2}LO. In the uncoupled $^3P_0$ wave, OPE is attractive and almost as strong as in the coupled $^3S_1$-$^3D_1$ channels: As we are going to see shortly, without counterterms spurious $^3P_0$ bound states start appearing for cutoff values which are only slightly larger than the ones spawning spurious states in the $^3S_1$-$^3D_1$ coupled channels [15]. The behavior in the coupled $^3P_2$-$^3F_2$ channels is similar to $^3S_1$-$^3D_1$, i.e., each of them contains one attractive and one repulsive eigenchannel. Spurious bound states appear in the $^3P_2$-$^3F_2$ channels for much larger cutoffs, meaning a weaker singular potential [15].

(3) The situation is less obvious for the D waves. As in other singlet channels, in $^1D_2$ OPE is not singular. In the uncoupled $^3D_2$ wave without counterterm, the spurious states appear after $^3P_0$ but before $^3P_2$-$^3F_2$ [15]. In contrast, the coupled $^3D_3$-$^3G_3$ channels are even less favorable to spurious states than $^3P_2$-$^3F_2$ [15,38]. This is consistent with the smallness of the $^3D_3$ phase shift at low energies. Still, the estimates from Ref. [25] clearly suggest the presence of nonperturbative pions in D waves. To be conservative, we treat OPE nonperturbatively in all D waves, which requires the additional LO counterterms $C_{^3D_2}$ and $C_{^3D_3}$, even though they would be expected only at N^{4}LO on the basis of NDA.

(4) Pion exchange is likely to be perturbative for $l \geqslant 3$ [39,40], where phase shifts are small. But if OPE is iterated, none of these waves (including $^3F_4$-$^3H_4$ and $^3G_4$ where OPE's tensor force is attractive) accommodate spurious bound states in the range of cutoff values we investigate below (up to 10 GeV). This is consistent with the corresponding weakness of OPE [25]. In the following, we study low-energy neutron-deuteron scattering including neutron-proton partial waves nonperturbatively up to total angular momentum $j = 4$, as in Ref. [38]. We will show that including such high-angular-momentum components in the low-energy three-nucleon system is unnecessary. By including them, we are merely keeping some contributions of higher order that do not introduce harmful cutoff dependence in the cutoff range we consider.

The solution of the dynamical equations involving the above potentials, which are highly singular, requires regularization. We replace the potential by a regularized one,

$$V^{(0)}(\boldsymbol{p}',\boldsymbol{p}) = V_{1\pi}^{(0)}(\boldsymbol{p}',\boldsymbol{p}) + V_{\rm ct}^{(0)}(\boldsymbol{p}',\boldsymbol{p}) \to V_\Lambda^{(0)}(\boldsymbol{p}',\boldsymbol{p}) = f_n(\boldsymbol{p}'/\Lambda)\,V^{(0)}(\boldsymbol{p}',\boldsymbol{p})\,f_n(\boldsymbol{p}/\Lambda), \quad (3)$$

with the regulator function $f_n(x)$ in form of exponentials,

$$f_n(x) = \exp(-x^n), \quad n = 2,4,6. \quad (4)$$

This form is easily decomposed into partial waves, ensuring no additional mixing among waves. We will use the regulator with $n = 4$, unless otherwise mentioned. Regulator (in)dependence will be discussed later.

We study the two-body system (neutron-proton scattering and deuteron bound state) by solving the LS equation for the LO T matrix,

$$T^{(0)}(\boldsymbol{p}',\boldsymbol{p}) = V_\Lambda^{(0)}(\boldsymbol{p}',\boldsymbol{p}) + \int d^3\boldsymbol{k}\; V_\Lambda^{(0)}(\boldsymbol{p}',\boldsymbol{k}) \times \frac{m_N}{\boldsymbol{p}^2 - \boldsymbol{k}^2 + i\epsilon} T^{(0)}(\boldsymbol{k},\boldsymbol{p}), \quad (5)$$

where $m_N = 938.9$ MeV is the nucleon mass. The on-shell amplitude $T(p)$ in a certain partial wave then gives the LO phase shift in that wave,

$$\delta^{(0)}(p) = -\frac{i}{2}\ln[1 - i\pi m_N p\, T^{(0)}(p)]. \quad (6)$$

There are many ways to fix the values of counterterms at each cutoff. In this work, we choose the following ways to determine them:

(1) All counterterms, except $C_{^3D_3}$, are fitted to PWA93 phase-shift data [41] at laboratory energy $T_L = 5$ MeV or 10 MeV. In contrast, the $^3D_3$ phase shifts are too small at low energies to perform a reliable fit. Therefore, for this wave we perform a global fit of phase shifts up to $T_L = 200$ MeV through χ^2 minimization, similar to the way it was done in Ref. [38].
(2) Alternatively, for S waves ($^1S_0$ or $^3S_1$) we may adjust the counterterms to reproduce singlet ($a_s = -23.75$ fm) and triplet ($a_t = 5.42$ fm) scattering lengths. Another option for the $^3S_1$ counterterm is to adjust it by fitting the deuteron binding energy.

We will discuss the dependence on the fitting method in detail in the next section. As we are going to see, renormalization guarantees that no bound states cross the zero-energy threshold, so phase shifts remain essentially cutoff independent. Instead, deep bound states, which are beyond the region of validity of the EFT, appear at certain cutoffs [15].

With the two-nucleon system properly renormalized, the three-nucleon system is studied by solving the Faddeev equations in configuration space with the LO EFT potential. In particular, we calculate the triton binding energy and neutron-deuteron scattering lengths. The configuration-space two-nucleon potential is obtained by carrying out a numerical Fourier transformation of its momentum-space counterpart. We remove the spurious deep two-body bound states by using an orthogonalizing pseudopotential technique; see Refs. [15,42]. That is, we replace the two-body potential,

$$V_\Lambda^{(0)} \to \tilde{V}_\Lambda^{(0)} = V_\Lambda^{(0)} + \sum_n |\psi_n\rangle \lambda_n \langle\psi_n|, \tag{7}$$

where the sum runs over the deep states with wave functions ψ_n, and λ_n are large (positive) numbers. A three-body force is not included in these calculations; instead, we analyze the cutoff dependence of three-body observables to check whether a three-body counterterm is missing at LO.

The three-body wave function, $\Psi^{(0)}$, is written in terms of Faddeev components, $\psi_k^{(0)}$,

$$\Psi^{(0)}(\boldsymbol{x},\boldsymbol{y}) = \psi_1^{(0)}(\boldsymbol{x}_1,\boldsymbol{y}_1) + \psi_2^{(0)}(\boldsymbol{x}_2,\boldsymbol{y}_2) + \psi_3^{(0)}(\boldsymbol{x}_3,\boldsymbol{y}_3), \tag{8}$$

where a set of Jacobi coordinates, defined by $\boldsymbol{x}_k = (\boldsymbol{r}_j - \boldsymbol{r}_i)$ and $\boldsymbol{y}_k = (2\boldsymbol{r}_k - \boldsymbol{r}_i - \boldsymbol{r}_j)/\sqrt{3}$ with particle indices $i,j,k = 1,2,3$, is used. Given isospin symmetry at LO, the three Faddeev equations become formally identical, and read

$$\left(E - H_0 - \tilde{V}_{\Lambda ij}^{(0)}\right)\psi_k^{(0)} = \tilde{V}_{\Lambda ij}^{(0)}\left(\psi_i^{(0)} + \psi_j^{(0)}\right), \tag{9}$$

where E is the three-body energy, H_0 is the three-particle kinetic energy operator in the center-of-mass frame, and $\tilde{V}_{\Lambda ij}^{(0)}$ is the LO two-body interaction between particles i and j. By using the operator P_{ij} for a permutation of particles i and j, the Faddeev components can also be written as

$$\psi_i^{(0)} + \psi_j^{(0)} = (P_{12}P_{23} + P_{23}P_{12})\psi_k^{(0)}. \tag{10}$$

The angular and spin-isospin dependence of the Faddeev components is described using a bipolar harmonic basis, and the partial Faddeev amplitude $F_\alpha(x_k, y_k)$ is defined from

$$\psi_k^{(0)}(\boldsymbol{x}_k,\boldsymbol{y}_k) = \sum_\alpha \frac{F_\alpha(x_k,y_k)}{x_k y_k} \left|\left[l_x(s_i s_j)_{s_x}\right]_{j_x}(l_y s_k)_{j_y}\right\rangle_{JM} \otimes \left|(t_i t_j)_{t_x} t_k\right\rangle_{TT_z}, \tag{11}$$

where the index α represents all allowed combinations of the quantum numbers present in the kets; s_i and t_i are, respectively, the spins and isospins of the individual particles; s_x and t_x are, respectively, the total spin and isospin of the two particles associated with the Jacobi coordinate x; l_x and l_y (j_x and j_y) are the orbital (total) angular momenta associated with the corresponding Jacobi coordinates; and J and M (T and T_z) are, respectively, the total angular momentum (isospin) and its third component. For neutron-deuteron scattering at zero energy, the Faddeev component satisfies the following boundary condition for $y_{\rm nd} \to \infty$:

$$\psi_{k_{\rm nd}=0}^{(0)}(\boldsymbol{x}_k,\boldsymbol{y}_k) = \sum_\alpha \frac{\delta_{l_y,0}}{\sqrt{3}}\left(1 - 2\frac{^{2J+1}a_{\rm nd}^{(0)}}{\sqrt{3}y_k}\right)\frac{f_\alpha^d(x_k)}{x_k} \times \left|\left[l_\alpha(s_i s_j)_{s_d}\right]_{j_d}(l_y s_k)_{j_k}\right\rangle_{JM} \otimes \left|(t_i t_j)_{t_d} t_k\right\rangle_{TT_z}, \tag{12}$$

where f_α^d is the deuteron's wave-function component for orbital angular-momentum component l_α dependent on coordinate $\boldsymbol{x}_k$; $s_d = 1$, $j_d = 1$, and $t_d = 0$ are, respectively, the deuteron's spin, angular momentum, and isospin; and $^{2J+1}a_{\rm nd}^{(0)}$ is the LO scattering length for either doublet ($J = 1/2$) or quartet ($J = 3/2$) channels. Details of the numerical methods employed here can be found in Refs. [43–45].

B. Next-to-leading order

By performing the renormalization procedure the essential cutoff dependence of observables is absorbed by counterterms. The effects of the residual cutoff dependence are comparable to the size of higher-order interaction terms. According to the analysis performed by Long and Yang [30], the LO residual cutoff dependence in the $^1S_0$ partial wave is $\propto Q/\Lambda$, and thus requires a counterterm at $\mathcal{O}(Q/M_{\rm hi})$. This is consistent with our numerical analysis of the residual cutoff dependence in $^1S_0$ phase shifts, shown below. The argument here is the same as used in Pionless EFT [10], while NDA would assign this counterterm to N^{2}LO.

Therefore, for RGI, we introduce a new counterterm in the $^1S_0$ channel at NLO, which gives rise to a short-range contribution to the effective range. We write the NLO two-nucleon potential as

$$V_{\rm ct}^{(1)}(\boldsymbol{p}',\boldsymbol{p}) = \frac{1}{(2\pi)^3}\left[\tilde{C}_{^1S_0}^{(1)} + \tilde{D}_{^1S_0}^{(1)}(p'^2 + p^2)\right]P_{^1S_0}, \tag{13}$$

where $\tilde{D}_{^1S_0}^{(1)}$ is the new counterterm needed at NLO, while $\tilde{C}_{^1S_0}^{(1)}$ is an NLO correction to the LO counterterm $\tilde{C}_{^1S_0}^{(0)}$. As before, we regulate the NLO potential,

$$V_{\rm ct}^{(1)}(\boldsymbol{p}',\boldsymbol{p}) \to V_\Lambda^{(1)}(\boldsymbol{p}',\boldsymbol{p}) = f_n(\boldsymbol{p}'/\Lambda)\, V_{\rm ct}^{(1)}(\boldsymbol{p}',\boldsymbol{p})\, f_n(\boldsymbol{p}/\Lambda), \tag{14}$$

with the regulator functions (4).

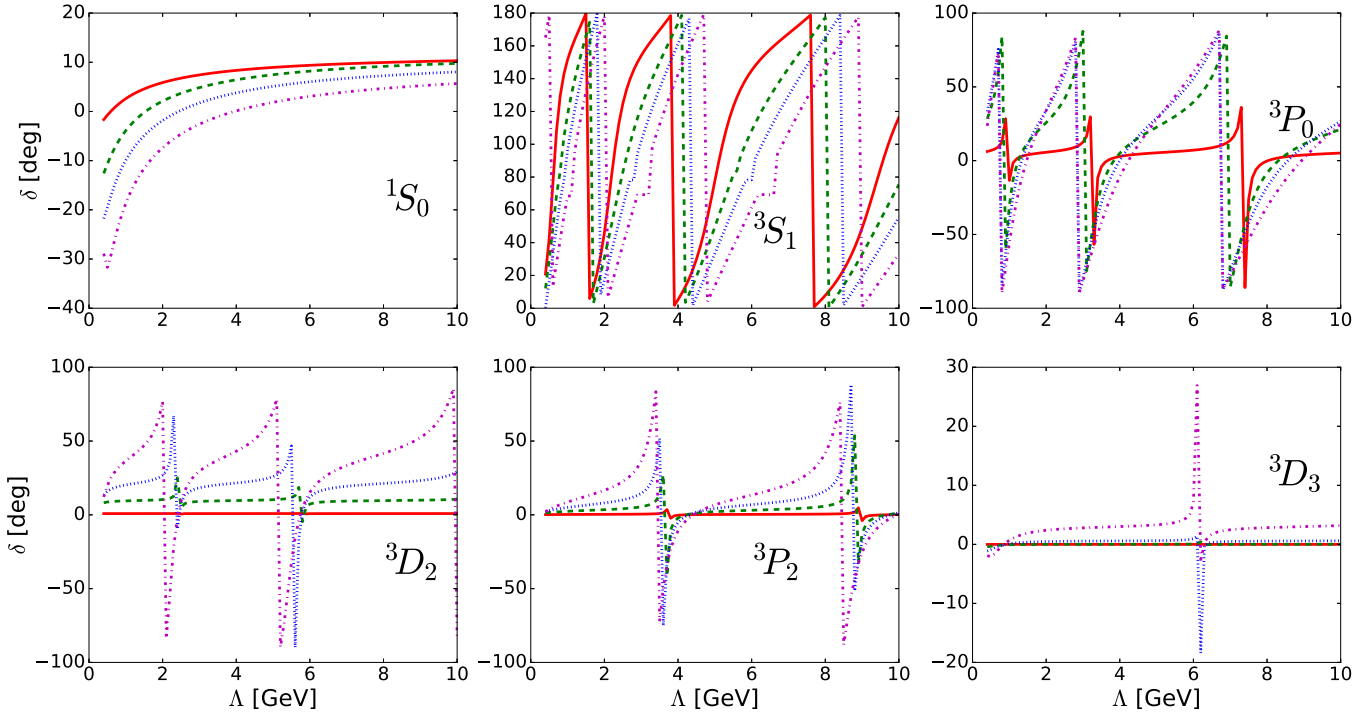

FIG. 1. Cutoff dependence of the phase shifts in $^1S_0$ and attractive tensor channels ($^3S_1$, $^3P_0$, $^3D_2$, $^3P_2$, $^3D_3$) without counterterms, with the $n = 4$ regulator. Results are given for different laboratory kinetic energies: 10 MeV (red solid line), 50 MeV (green dashed line), 100 MeV (blue dotted line), and 200 MeV (magenta dot-dashed line).

While we compute the LO T matrix $T^{(0)}$ nonperturbatively by solving the LS equation with the LO potential, we obtain the perturbative NLO correction $T^{(1)}$ using the distorted-wave Born approximation (DWBA) [30],

$$T^{(1)}(\boldsymbol{p}',\boldsymbol{p}) = V_\Lambda^{(1)}(\boldsymbol{p}',\boldsymbol{p}) - \int d^3\boldsymbol{k}\, \frac{m_N}{\boldsymbol{k}^2 - \boldsymbol{p}^2 - i\epsilon} \times \left[V_\Lambda^{(1)}(\boldsymbol{p}',\boldsymbol{k})T^{(0)}(\boldsymbol{k},\boldsymbol{p}) + T^{(0)}(\boldsymbol{p}',\boldsymbol{k})V_\Lambda^{(1)}(\boldsymbol{k},\boldsymbol{p})\right] + \int d^3\boldsymbol{k}' \int d^3\boldsymbol{k}\, T^{(0)}(\boldsymbol{p}',\boldsymbol{k}')\frac{m_N}{\boldsymbol{k}'^2 - \boldsymbol{p}^2 - i\epsilon} \times V_\Lambda^{(1)}(\boldsymbol{k}',\boldsymbol{k})\frac{m_N}{\boldsymbol{k}^2 - \boldsymbol{p}^2 - i\epsilon}T^{(0)}(\boldsymbol{k},\boldsymbol{p}). \quad (15)$$

The NLO correction to the $^1S_0$ phase shift, $\delta^{(1)}$, is then obtained from the on-shell amplitude by

$$\delta^{(1)}(p) = -\frac{\pi m_N p}{2}\mathrm{Re}[e^{-2i\delta^{(0)}(p)}\, T^{(1)}(p)], \quad (16)$$

where $\delta^{(0)}$ is the LO phase shift (6).

For a given LO counterterm $\tilde{C}^{(0)}_{^1S_0}$, the NLO counterterm $\tilde{D}^{(1)}_{^1S_0}$ is determined by fitting the PWA93 phase shift at a different energy or, alternatively, the effective range ($r_s = 2.77$ fm). The NLO counterterm $\tilde{C}^{(1)}_{^1S_0}$ ensures that the NLO correction vanishes for the observables used in fitting the LO counterterm.

NLO corrections to three-body observables are calculated in first-order perturbation theory. The correction to the three-body binding energy is

$$\Delta E^{(1)} = \langle\Psi^{(0)}|\sum_{ij} V^{(1)}_{\Lambda ij}|\Psi^{(0)}\rangle, \quad (17)$$

where $\Psi^{(0)}$ is the normalized three-body bound-state wave function due to LO potential. Similarly, for the correction to the scattering length,

$$\Delta a^{(1)}_{\mathrm{nd}} = \sqrt{\frac{3}{4}}\frac{m_N}{\hbar^2}\langle\Psi^{(0)}_{k_{\mathrm{nd}}=0}|\sum_{ij} V^{(1)}_{\Lambda ij}|\Psi^{(0)}_{k_{\mathrm{nd}}=0}\rangle, \quad (18)$$

where $\Psi^{(0)}_{k_{\mathrm{nd}}=0}$ is the LO three-body wave function for neutron-deuteron scattering at zero energy which is normalized to have unit flux as Eq. (12).

We emphasize that NLO is strictly treated as a perturbation, i.e., one insertion of the NLO potential (14). This is done regardless of the size of the NLO potential relative to LO, which is not an observable since both potentials are singular and cutoff dependent. A perturbative calculation, of course, does not reflect the results of an exact solution of the LS and Faddeev equations with the sum of LO and NLO potentials. An exact solution includes all insertions of the NLO potential but not the associated counterterms, so it leads, in general, to a nonrenormalizable amplitude. For example, two insertions of the NLO potential are an N^{2}LO effect, whose renormalization requires an N^{2}LO interaction with four powers of momenta. The latter is missing if we iterate the NLO potential. In Pionless EFT, it can be shown analytically that the two-body amplitude is not renormalizable for positive effective range if the NLO potential is treated exactly [46], a manifestation of Wigner's

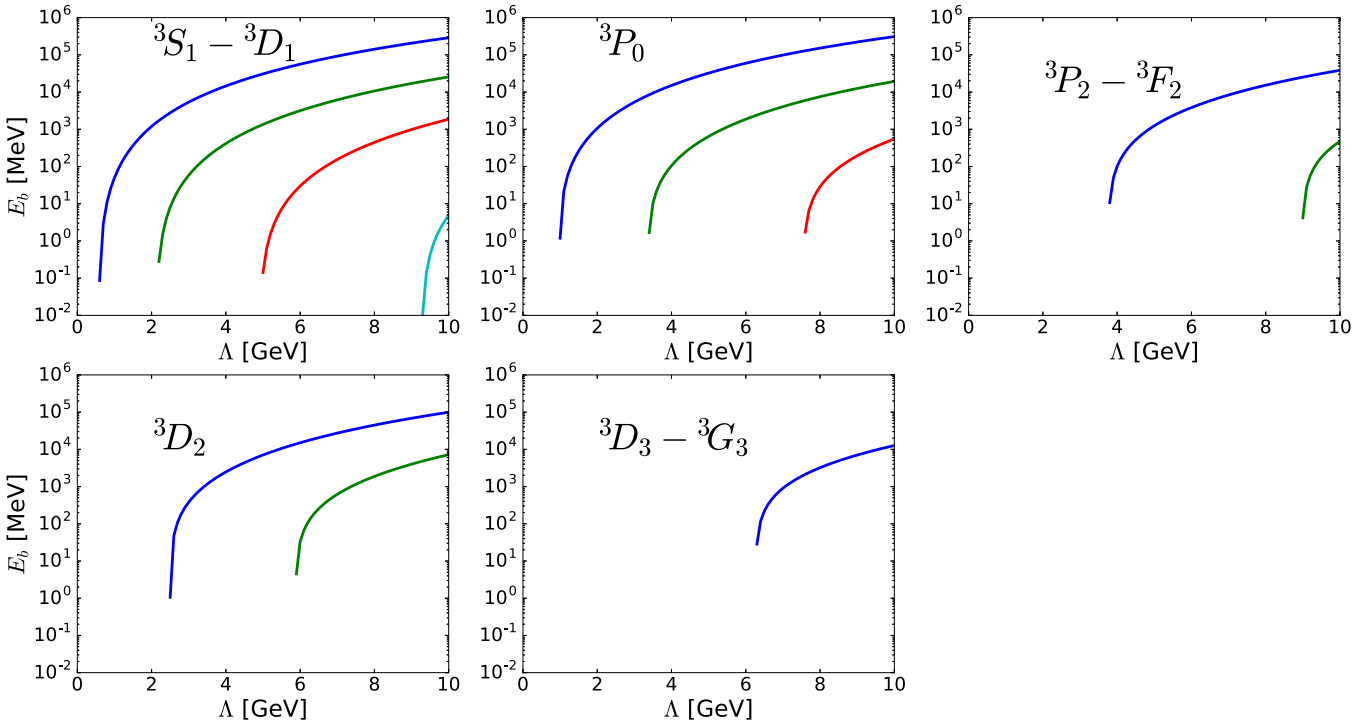

FIG. 2. Cutoff dependence of the binding energies of unphysical bound states in attractive tensor channels without counterterms, with the $n = 4$ regulator.

bound [47]. Thus, renormalization at the two-nucleon level forces us here, as in Pionless EFT [48–50], into a perturbative evaluation of NLO corrections in few-body systems.

As in any perturbation theory, the DWBA calculation of the NLO T matrix will explicitly break the unitarity of the S matrix. The definition of the phase shift we use [Eq. (16)] is

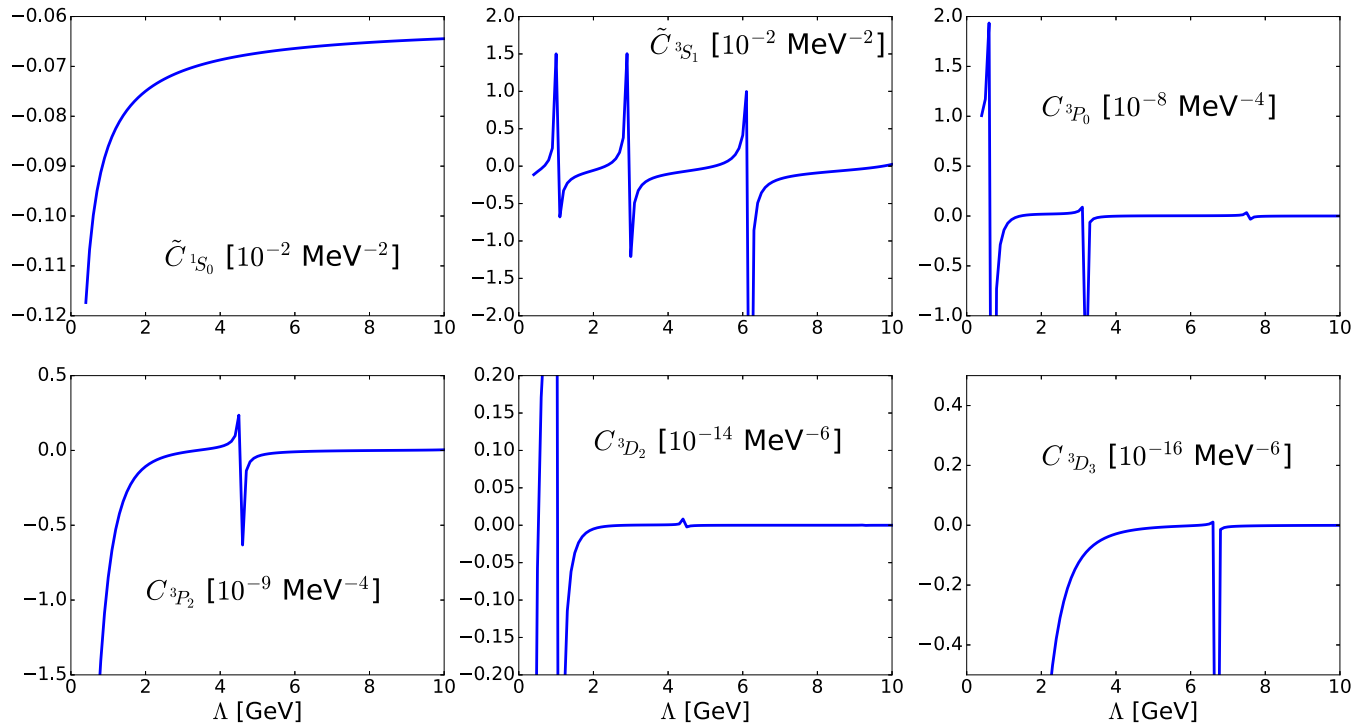

FIG. 3. Cutoff dependence of LO counterterms with the $n = 4$ regulator. Counterterms are fitted to PWA93 phase shifts at 10 MeV, except for the $^3D_3$ channel, which is globally fitted to phase shifts up to 200 MeV.

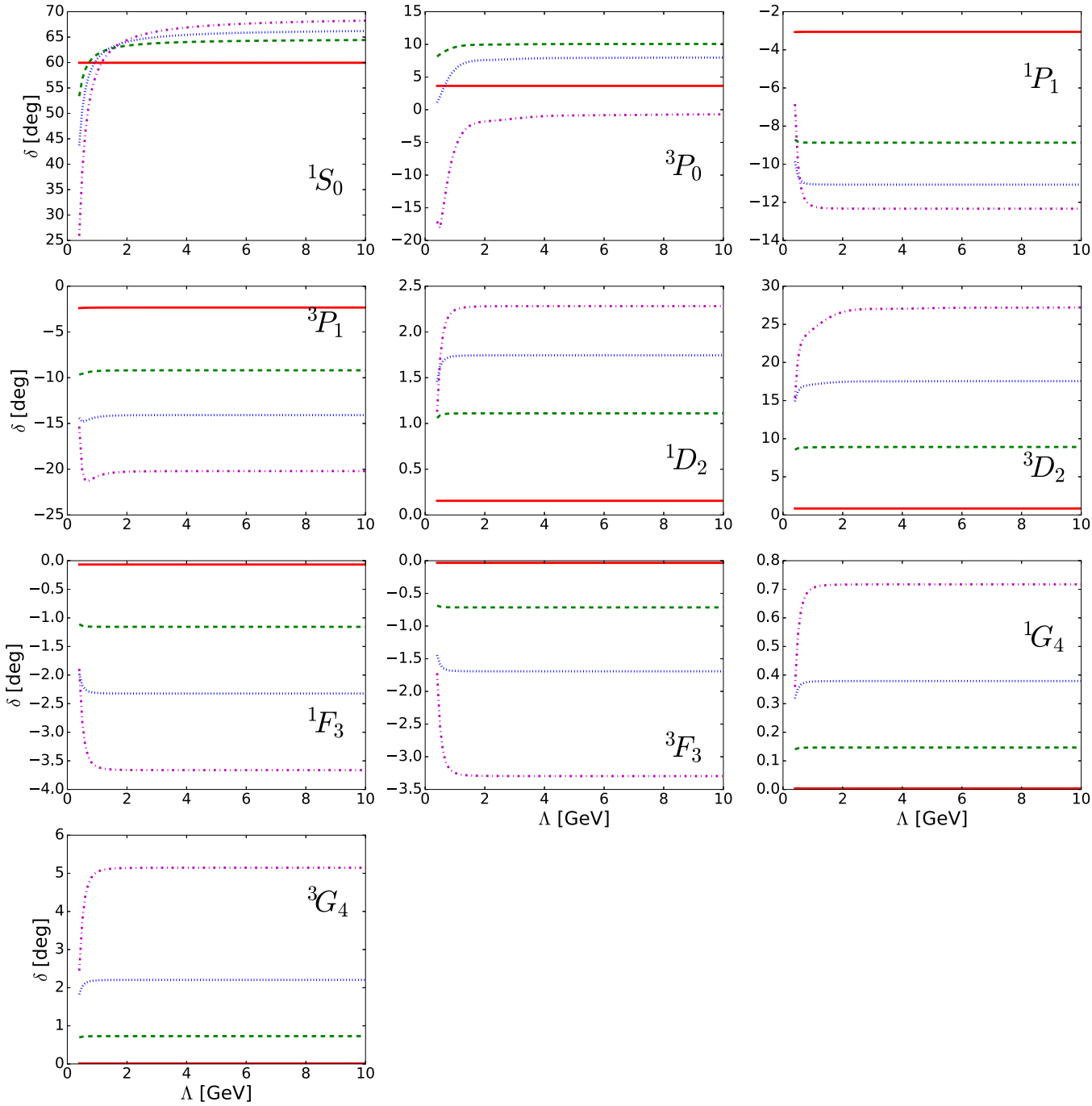

FIG. 4. Cutoff dependence of LO phase shifts in uncoupled channels up to total angular momentum $j = 4$, with the $n = 4$ regulator. Curves as in Fig. 1.

not unique. However, the error coming from the breaking of unitarity, or alternatively from different definitions of the NLO phase shift, can be considered an N^{2}LO effect. The amount of this breaking is one of the components of our total NLO error. While the difference between LO and NLO seems considerable at the level of the $^1S_0$ phase shifts, we are going to see only relatively minor changes in the three-body observables we calculate. Were this not the case, we would have been forced to consider an even larger departure from NDA: We would have to elevate $^1S_0$ range effects to LO, which at present can be done without violation of RGI only through a dibaryon field [51].

III. RESULTS

A. Two-nucleon system at LO

In order to understand the effects of the counterterms at LO, we study neutron-proton scattering phase shifts and the deuteron binding energy. Phase shifts and their cutoff dependence are obtained by solving the LS equation in each

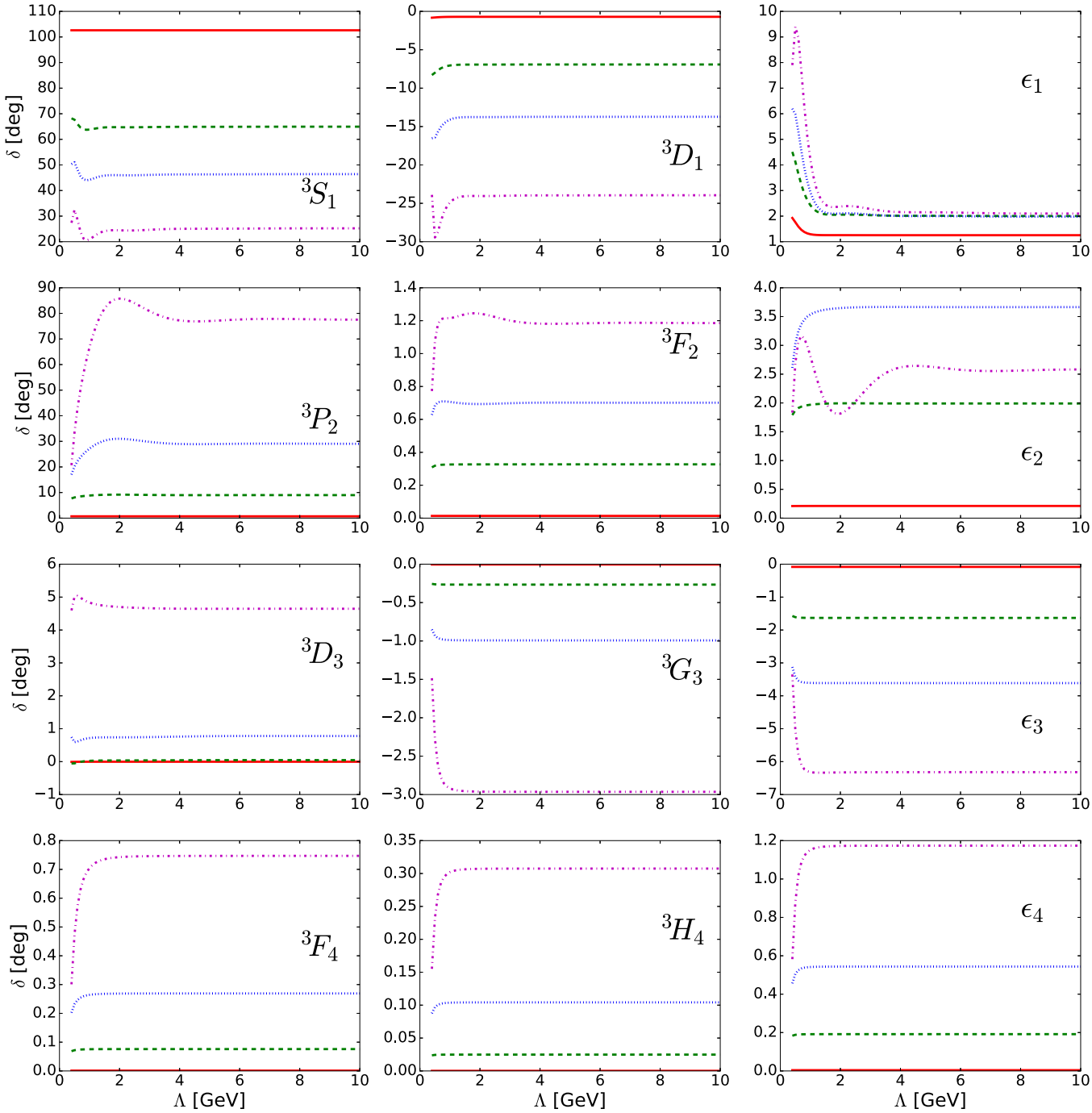

FIG. 5. Cutoff dependence of LO phase shifts in coupled channels up to total angular momentum $j = 4$, with the $n = 4$ regulator. Curves as in Fig. 1.

partial wave with the LO Chiral EFT potential as an input. The results of Ref. [15] are reproduced with cutoffs up to 4 GeV, and the cutoff range is extended to 10 GeV. Our results are similar to those reported in Refs. [38,52].

We plot the cutoff dependence of selected np phase shifts in Fig. 1 for a pure OPE potential, with the $n = 4$ regulator (4) but without any counterterm. The $^1S_0$ phase shift is typical of other singlet channels in that it converges as the cutoff increases. Phase shifts in triplet channels where the OPE tensor force is repulsive also converge, but in those where the tensor force is attractive ($^3S_1$, $^3P_0$, $^3P_2$, $^3D_2$, $^3D_3$) oscillations covering the range of phase shift values are seen. These oscillations are a reflection of bound states crossing threshold, as observed in Fig. 2 where the cutoff dependence of binding energies is displayed.

As noted in Ref. [15], the appearance of unphysical bound states is due to the singular nature of the OPE potential in the attractive tensor channels. To achieve RGI, one is obliged to introduce counterterms at LO in these channels. In $^3S_1$, the counterterm is the one prescribed by NDA, but counterterms

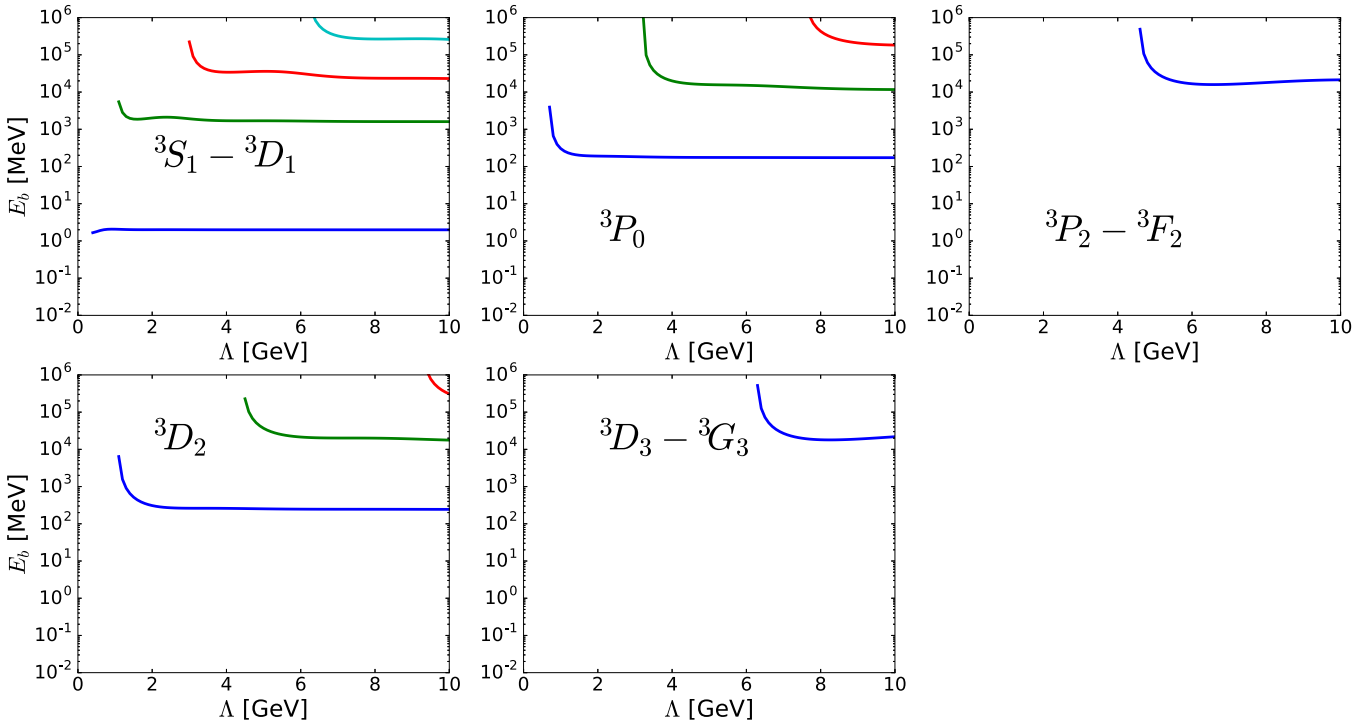

FIG. 6. Cutoff dependence of binding energies in attractive tensor channels after including a counterterm in each channel, with the $n = 4$ regulator.

are needed in all attractive tensor channels where pions are treated nonperturbatively. Other channels do not contain spurious bound states and reveal moderate cutoff dependence in phase shifts up to $\Lambda \sim 10$ GeV. Nevertheless, in $^1S_0$ a counterterm is suggested by NDA and should also be included, since there seems to be no argument for its demotion from LO.

Once the counterterms in attractive tensor channels are included at LO, they can be fitted to reproduce PWA93 phase shifts at low energy. In Fig. 3, the cutoff dependence of the counterterms, which are fitted to PWA93 at a laboratory energy of 10 MeV (except for the $^3D_3$ channel which is fitted globally), is presented.

Because the counterterms absorb most of the cutoff dependence in phase shifts, we now observe convergence at large cutoff values. Figures 4 and 5 show the residual cutoff dependence of phase shifts in uncoupled and coupled channels, respectively. As expected in an EFT, the residual cutoff dependence is largest at the largest energies. For cutoff values larger than 2 GeV, the bulk of the low-energy phase shifts becomes cutoff independent. The mixing angle ϵ_2 at $T_L = 150$ MeV retains the strongest cutoff dependence; nevertheless, it becomes pretty small for $\Lambda \gtrsim 4$ GeV. Note that the $^3F_4$-$^3H_4$ coupled channels, dominated by the strong centrifugal barrier, do not require any counterterm up to $\Lambda \sim 10$ GeV: They show essentially no cutoff dependence, regardless of the fact that it is an attractive tensor channel. Of course, were the cutoff to be increased further, cutoff dependence would eventually appear. To investigate observables at such cutoff values one should include another LEC or, more appropriately, treat OPE in these channels as a subleading correction, that is, in DWBA.

After the renormalization procedure, the cutoff dependence of the binding energies of spurious bound states also changes completely; see Fig. 6. Only a single low-energy bound state appears, the deuteron in the $^3S_1$ channel, and its binding energy is nearly cutoff independent. Deep bound states exist, which also converge as the cutoff increases, but they correspond to states outside the applicability of EFT. These unphysical states must be removed when considering the three-nucleon problem. Turning the binding energy of the shallowest of these states, the least-bound $^3P_0$ state ($\approx$170 MeV), into an estimate of the breakdown scale, we find $M_{\rm hi} \sim 400$ MeV. This is somewhat low, but a better estimate requires a careful study of the convergence of observables with order in the EFT expansion.

The energy dependence of the LO phase shifts in each partial wave is shown in Fig. 7 for uncoupled channels and in Fig. 8 for coupled channels. The largest deviation in comparison with PWA93 is in the $^1S_0$ partial wave, for which corrections appear at NLO. As we will see later, this deviation is indeed mitigated at NLO.

RGI requires not only independence of observables on the numerical value of the cutoff Λ but also independence on the form of the regulator function itself. In Fig. 9, the cutoff dependence of phase shifts is compared for the regulator functions $f_n(x)$ in Eq. (4) with $n = 2,4,6$. Dependence on the regulator function becomes negligible for large cutoffs but, as expected, it is still relevant at small cutoff values. The regulator-function dependence is in all cases not larger than the Λ variation for each regulator in the region $\Lambda \gtrsim 1$ GeV. Our results demonstrate that at large cutoff values phase shifts become essentially independent of the choice of regulator function.

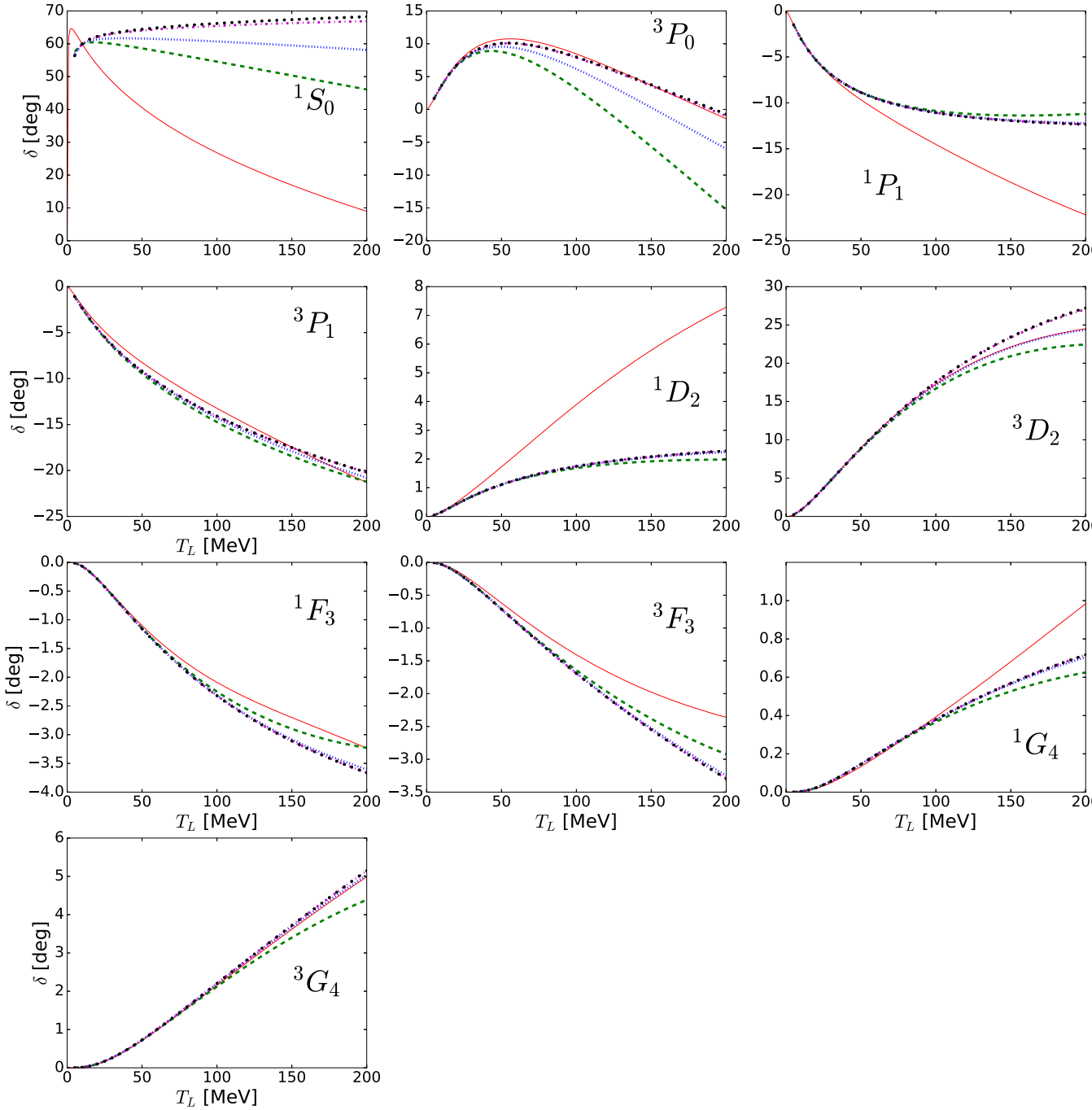

FIG. 7. Laboratory energy dependence of LO phase shifts in uncoupled channels up to $j = 4$, with the $n = 4$ regulator. Results are given for cutoff values of 600 MeV (green dashed line), 1 GeV (blue dotted line), 4 GeV (magenta dot-dashed line), and 10 GeV (black dots), and compared with PWA93 data (red solid line).

More generally, RGI ensures that physical observables are insensitive to the arbitrary separation of long-range and short-range dynamics. Because the long-range part of the potential is dominated by the OPE interaction, we can expect insensitivity to details of the fitting procedure, as long as they are used to reproduce low-energy observables. In this work, we check the sensitivity on the fitting procedure by comparing results with counterterms that are fitted at different energies, with the $n = 4$ regulator. Table I lists our four fitting choices, labeled (I)–(IV).

The $^3P_0$, $^3P_2$, and $^3D_2$ counterterms are fitted to PWA93 phase shifts at $T_L = 5$ MeV or 10 MeV. Figure 10 shows a comparison of the cutoff dependence for $l > 0$ phase shifts at several energies, for fitting procedures (I) and (II). The $^1S_0$ and $^3S_1$ counterterms are fitted to phase shifts at $T_L = 5$ or 10 MeV, or to scattering lengths or (for $^3S_1$) the deuteron

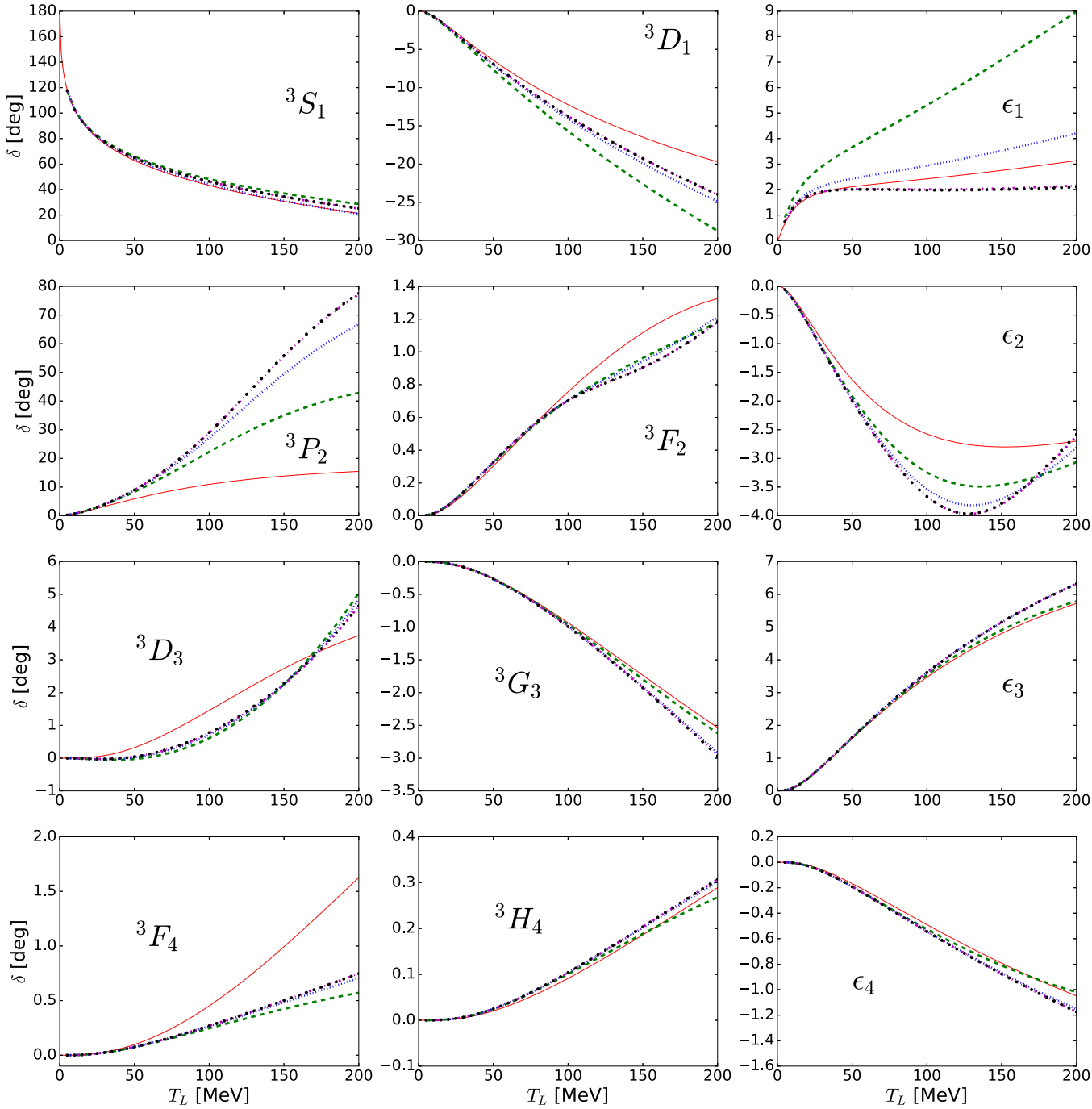

FIG. 8. Laboratory energy dependence of LO phase shifts in coupled channels up to $j = 4$, with the $n = 4$ regulator. Curves as in Fig. 7.

binding energy. Figure 11 shows the $^3S_1$ phase shifts as a function of the cutoff with counterterms fitted following strategies (I)–(IV), while Fig. 12 shows the analogous results for the $^1S_0$ phase shifts for strategies (I)–(III). Though all cases show cutoff independence at large cutoff values, the low-energy $^1S_0$ phase shifts are somewhat sensitive to the fitting method. This is because of the large deviation of the LO phase shift from PWA93 data in $^1S_0$ even at low energies. This uncertainty is expected to be reduced once higher-order corrections are included. For all other channels, the fitting procedure has very little impact on the phase shifts. This impact increases with energy but is not larger than the cutoff variation for $\Lambda \gtrsim 1$ GeV.

The residual cutoff dependence may be related to the order of missing higher-order corrections. As an example, let us consider the cutoff dependence of the $^1S_0$ scattering length in the cutoff range $\Lambda \geqslant 1.2$ GeV for the $n = 4$ regulator, when the counterterm is fitted to the phase shift at $T_L = 5$ MeV. We fit the cutoff dependence with a power series

$$a_s^{(0)}(\Lambda) = a_s^{(0)}(\infty)\left[1 + \frac{p_{s1}^{(0)}}{\Lambda} + \left(\frac{p_{s2}^{(0)}}{\Lambda}\right)^2 + \left(\frac{p_{s3}^{(0)}}{\Lambda}\right)^3 + \cdots\right], \quad (19)$$

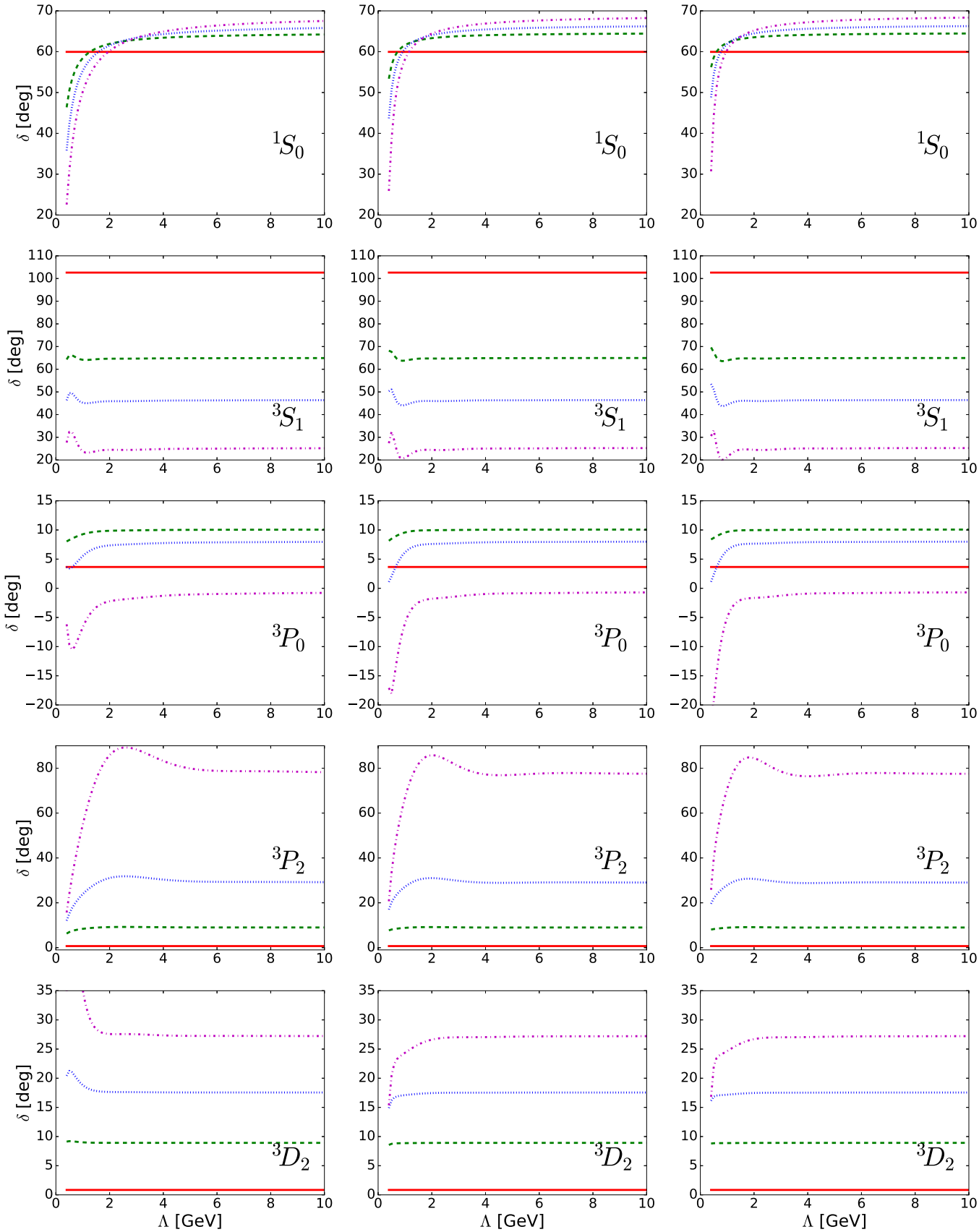

FIG. 9. Cutoff dependence of selected LO phase shifts for different regulators. Left, middle, and right graphs correspond to regulators in Eq. (4) with, respectively, $n = 2,4,6$. Curves as in Fig. 1.

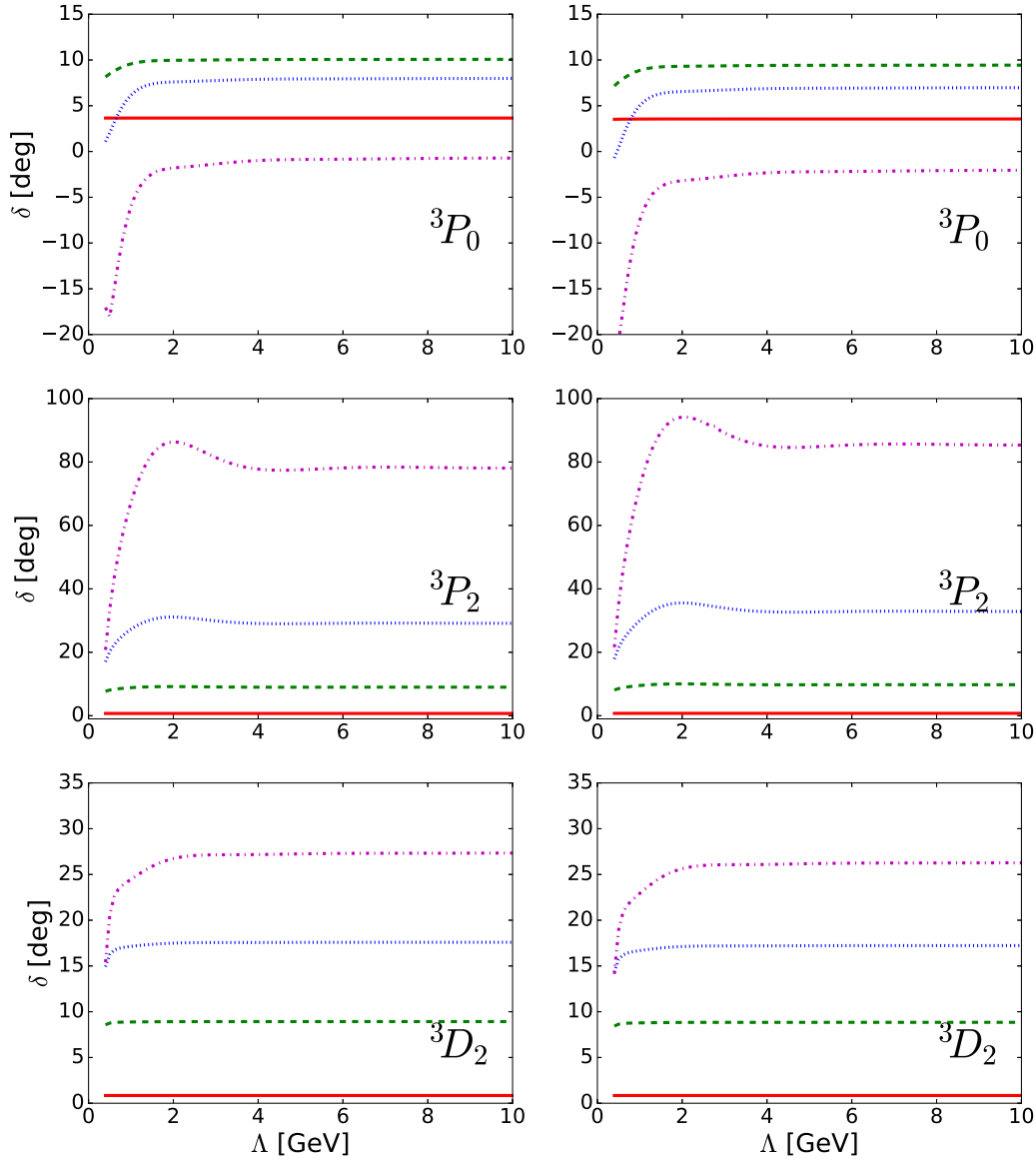

FIG. 10. Cutoff dependence of LO phase shifts for $l > 0$ partial waves with the $n = 4$ regulator, for different fitting energies. The graphs on the left column are obtained with counterterms fitted at $T_L = 10$ MeV and those on the right column with counterterms fitted at $T_L = 5$ MeV. Curves as in Fig. 1.

TABLE I. The four choices of fitting procedure employed in this work at LO and NLO, for $^1S_0$, $^3S_1$, and $l > 0$ counterterms. δ_E represents the PWA93 phase shift at kinetic energy E MeV; $a_{s,t}$ (r_s) stands for the singlet and triplet scattering lengths (singlet effective range); and E_d is deuteron binding energy. In all cases, the $^3D_3$ counterterm is determined by a global χ^2 minimization for phase shifts up to 200 MeV.

Index	$^1S_0$ LO	$^3S_1$ LO	$l > 0$ LO	$^1S_0$ NLO
(I)	δ_{10}	δ_{10}	δ_{10}	δ_{10},δ_{20}
(II)	δ_5	δ_5	δ_5	δ_5,δ_{10}
(III)	a_s	a_t	δ_{10}	a_s, r_s
(IV)	a_s	E_d	δ_5	a_s, r_s

truncating the series at successively larger powers. The fitting parameters $a_s^{(0)}(\infty)$ and $p_{s1,2,3}^{(0)}$ are summarized in Table II and the corresponding fits are shown in the left panel of Fig. 13. (Results are similar for other cutoff ranges, regulators, and fitting strategies.) The parameters are relatively stable as the number of fit parameters increases. For the four-parameter fit, the parameters $a_s^{(0)}(\infty)$ and $p_{s1,2}^{(0)}$ have nearly converged (within errors), while the large $p_{s3}^{(0)}$ error suggests that fits with more parameters are meaningless.

As expected, the momenta $p_{s1,2,3}^{(0)}$ are given by low-energy scales: While $p_{s2,3}^{(0)} \sim m_\pi$, $p_{s1}^{(0)}$ is somewhat smaller, possibly as a consequence of the fine tuning in this channel, but definitely nonvanishing. The residual cutoff dependence $\propto \Lambda^{-1}$ is consistent with the argument in Ref. [30], which implies a $Q/M_{\rm hi}$ counterterm. Also, note that with this input the LO

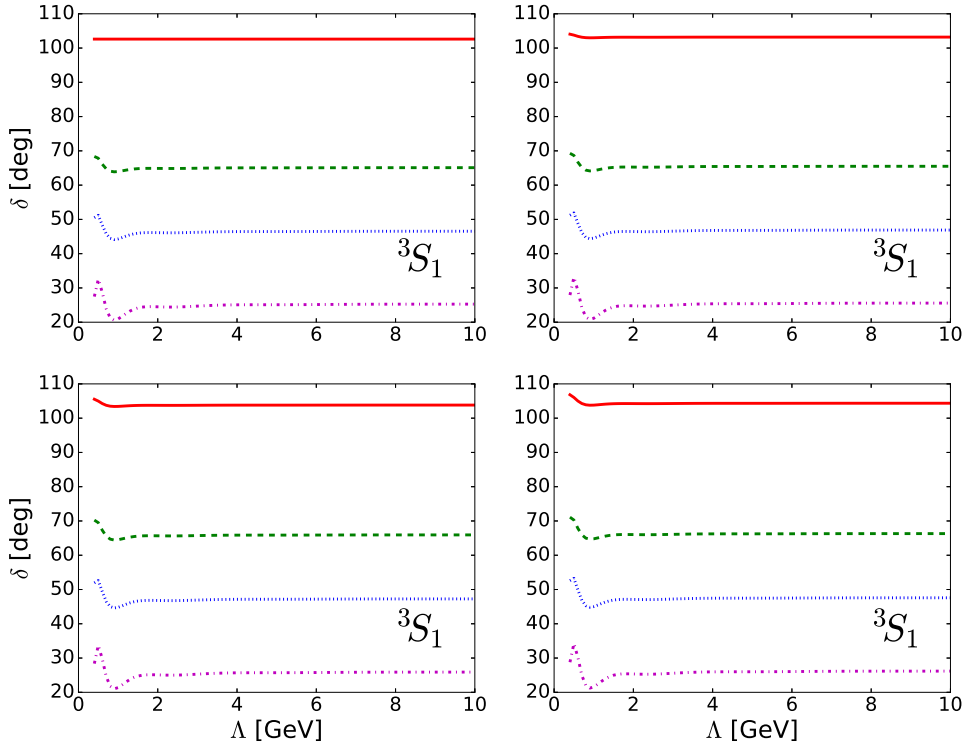

FIG. 11. Cutoff dependence of the LO $^3S_1$ phase shift with the $n = 4$ regulator, for different fitting methods. Graphs are obtained with counterterms fitted to PWA93 phase shifts at 10 MeV (upper left) or 5 MeV (upper right), to the scattering length (lower left), and to the deuteron binding energy (lower right). Curves as in Fig. 1.

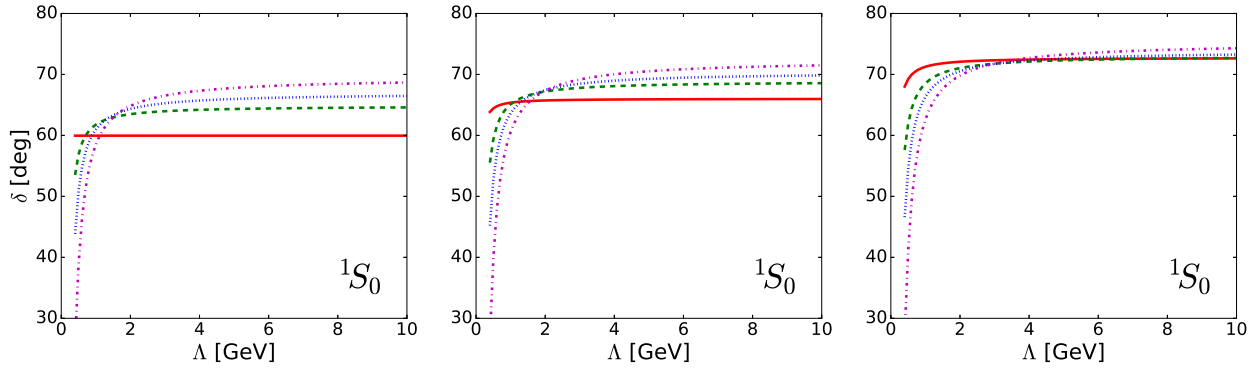

FIG. 12. Cutoff dependence of the LO $^1S_0$ phase shift with the $n = 4$ regulator, for different fitting methods. Graphs are obtained with counterterms fitted to PWA93 phase shifts at 10 MeV (left) or 5 MeV (middle) and to the scattering length (right). Curves as in Fig. 1.

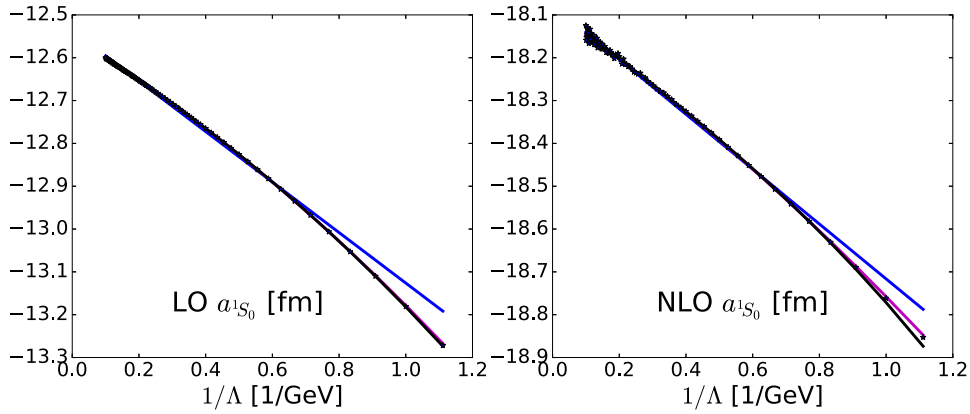

FIG. 13. Cutoff dependence of the $^1S_0$ scattering length at LO (left) and NLO (right) with the $n = 4$ regulator and fitting procedure (II). The blue, magenta, and black solid lines are, respectively, two-, three-, and four-parameter fits with Eqs. (19) and (22) to results for $\Lambda \geqslant 1.2$ GeV.

TABLE II. Parameters of fits using Eqs. (19) and (22) to the leading-order and next-to-leading-order results for the $^1S_0$ scattering length from fitting procedure (II) for cutoff values $\Lambda \geqslant 1.2$ GeV. The parameters $a_s^{(m)}(\infty)$ and $p_{s1,2,3}^{(m)}$ $(m = 0,1)$ are in fm and MeV, respectively. Numbers in parentheses represent fitting errors.

LO				NLO			
$a_s^{(0)}(\infty)$	$p_{s1}^{(0)}$	$p_{s2}^{(0)}$	$p_{s3}^{(0)}$	$a_s^{(1)}(\infty)$	$p_{s1}^{(1)}$	$p_{s2}^{(1)}$	$p_{s3}^{(1)}$
−12.5	47.0(0.3)			−18.1	35.4(0.3)		
−12.6	37.5(0.1)	111(11)		−18.1	30.2(0.9)	83(34)	
−12.6	38.3(0.3)	100(28)	124(86)	−18.1	32.5(2.8)	8(88)	176(183)

potential does not reproduce the scattering length—that is, the long-range component of the wave function—well. The introduction of an NLO correction will give more accurate values for the scattering length and the effective range.

In summary, our two-nucleon results are consistent with the results of Ref. [15] and also demonstrate that regulator independence is obtained up to cutoff values as large as 10 GeV for all partial waves. We turn now to the LO cutoff dependence of three-nucleon low-energy observables.

B. Three-nucleon system at LO

In order to check the cutoff dependence of the three-nucleon system with the LO Chiral EFT potential, we calculate neutron-deuteron scattering lengths and the triton binding energy by solving the Faddeev equation in configuration space. The two-nucleon EFT potential at LO is Fourier-transformed numerically from momentum space. There appears a small oscillating cutoff dependence in three-body results at large cutoff values. Similar oscillations also show up in the deuteron binding energy when calculated in configuration space; see Fig. 14. These oscillations are absent if the deuteron binding energy is calculated directly in momentum space and thus can be attributed to errors in the numerical Fourier transformation.

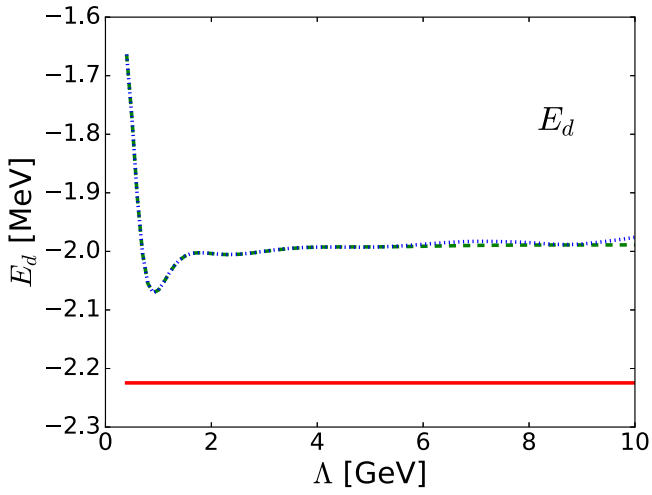

FIG. 14. Cutoff dependence of the LO deuteron energy with the $n = 4$ regulator. Results are shown for momentum-space (green dashed line) and configuration-space (blue dotted line) calculations, in comparison with experiment (red solid line).

Figure 15 shows the cutoff dependence of the triton binding energy and neutron-deuteron scattering lengths in doublet and quartet channels, when they are computed using the LO potential with counterterms fitted at $T_L = 10$ MeV and the $n = 4$ regulator. To see the three-nucleon effects of two-nucleon partial waves, we introduce a maximum total two-nucleon angular momentum $j_{\max}$ in the two-nucleon interaction, such that $\tilde{V}_{\Lambda ij}^{(0)}(\boldsymbol{x}) = 0$ if $j_x > j_{\max}$. Variation of $j_{\max}$ from 1 to 4 indicates that adding two-nucleon partial waves leads to small effects, which are negligible for $j_{\max} \geqslant 2$. This is consistent with the perturbativeness of $l \geqslant 3$ two-nucleon partial waves. For definiteness, below we show results for $j_{\max} = 4$. We see that cutoff independence is achieved in low-energy three-body observables: They vary by less than about 10% for $\Lambda \gtrsim 2$ GeV.

In addition, three-nucleon observables are insensitive to the form of the regulator, Eq. (4), as shown in Fig. 16. Essentially the same converged values are achieved regardless of the regulator choice, although as expected there is some regulator dependence at low cutoff values. The larger oscillations of $n = 6$ results can be attributed to artifacts from the numerical Fourier transformation.

We find that the triton is underbound and the nd scattering length in the doublet channel is rather large when compared to experiment. This is consistent with the underbinding of the deuteron and the poor description of $^1S_0$ phase shifts at LO. Thus, we compare results from the different choices of fitting procedure for S-wave counterterms shown in Table I. Figure 17 shows that cutoff independence is achieved for the three-nucleon system in all cases, but with some dependence on the counterterm fitting method. This dependence is comparable to the variation coming from cutoff values $\Lambda \gtrsim 1$ GeV. The deuteron binding energy and the nd quartet scattering length are closely correlated with the $^3S_1$ counterterm. As the latter changes to provide more attraction, the nd quartet scattering length decreases and crosses the experimental value. The triton binding energy and the nd doublet scattering length also approach experimental values, but remain quite far.

We observe in our results a correlation between the triton binding energy and the nd doublet scattering length known as the Phillips line [53]. It has been observed that different models tend to align in the plane generated by all values of the triton binding energy and the nd doublet scattering length. In our case, experimental values for these quantities are obtained at low cutoff values (less than 1 GeV), but are overshot by converged values. In contrast, the deuteron energy and the nd quartet scattering length initially approach the

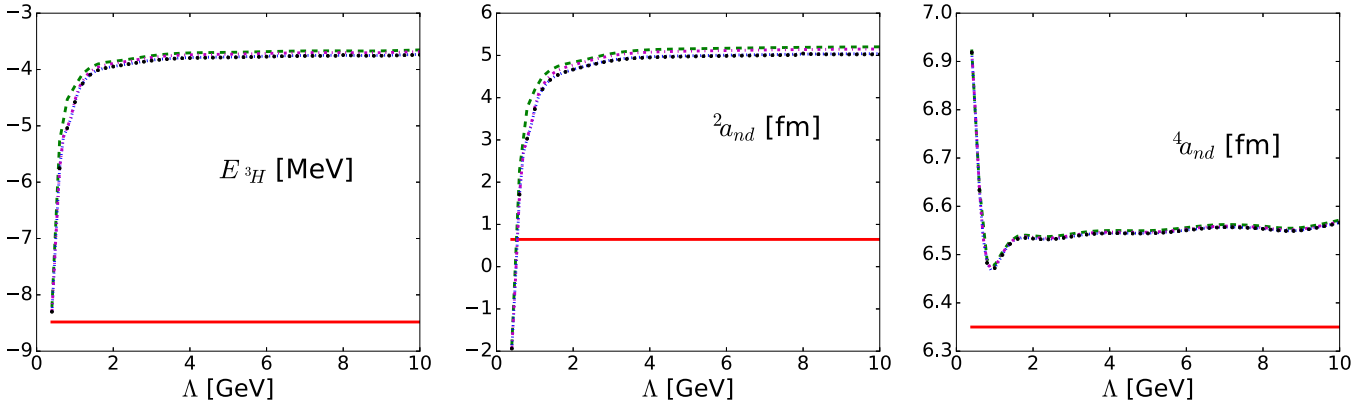

FIG. 15. Cutoff dependence of the triton energy (left), and $J = 1/2$ (middle) and $J = 3/2$ (right) neutron-deuteron scattering lengths at LO, for the $n = 4$ regulator. Results are shown for various $j_{\max}$ values in the two-nucleon interaction: $j_{\max} = 1$ (green dashed line), $j_{\max} = 2$ (blue dotted line), $j_{\max} = 3$ (magenta dot-dashed line), and $j_{\max} = 4$ (black dots), in comparison with experiment (red solid line).

experimental values but never reach them. Our unconverged results can be seen as models that should produce a Phillips line as the cutoff is varied. The left panel of Fig. 18 shows this correlation at LO, together with model calculations. The arrow in the graph indicates the direction of increasing cutoff. Note that only the end point of each line is our final result in the cutoff-independent limit. The spread of lines around these points gives a lower bound on the expected contribution from the next order. It is understandable that strategy (IV) is closest to the phenomenological Phillips line, since phenomenological models are usually made to reproduce the two-nucleon effective-range parameters, which determines the slope of the line.

The cutoff dependence of three-body observables suggests that, unlike the Pionless EFT case, there is no need for a three-body force at LO. This is consistent with Weinberg's

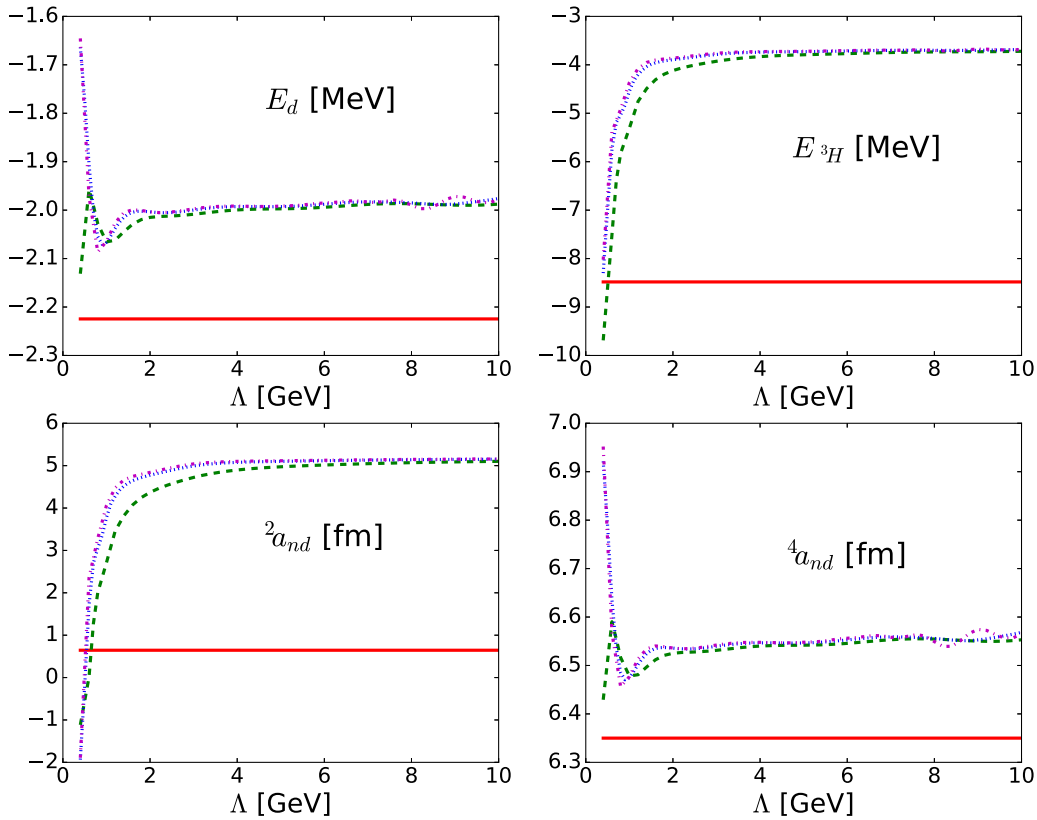

FIG. 16. Cutoff dependence of deuteron (top left) and triton (top right) energies, and $J = 1/2$ (bottom left) and $J = 3/2$ (bottom right) neutron-deuteron scattering lengths at LO, for different regulator choices, Eq. (4). Results are shown for $n = 2$ (green dashed line), $n = 4$ (blue dotted line), and $n = 6$ (magenta dot-dashed line), in comparison with experiment (red solid line).

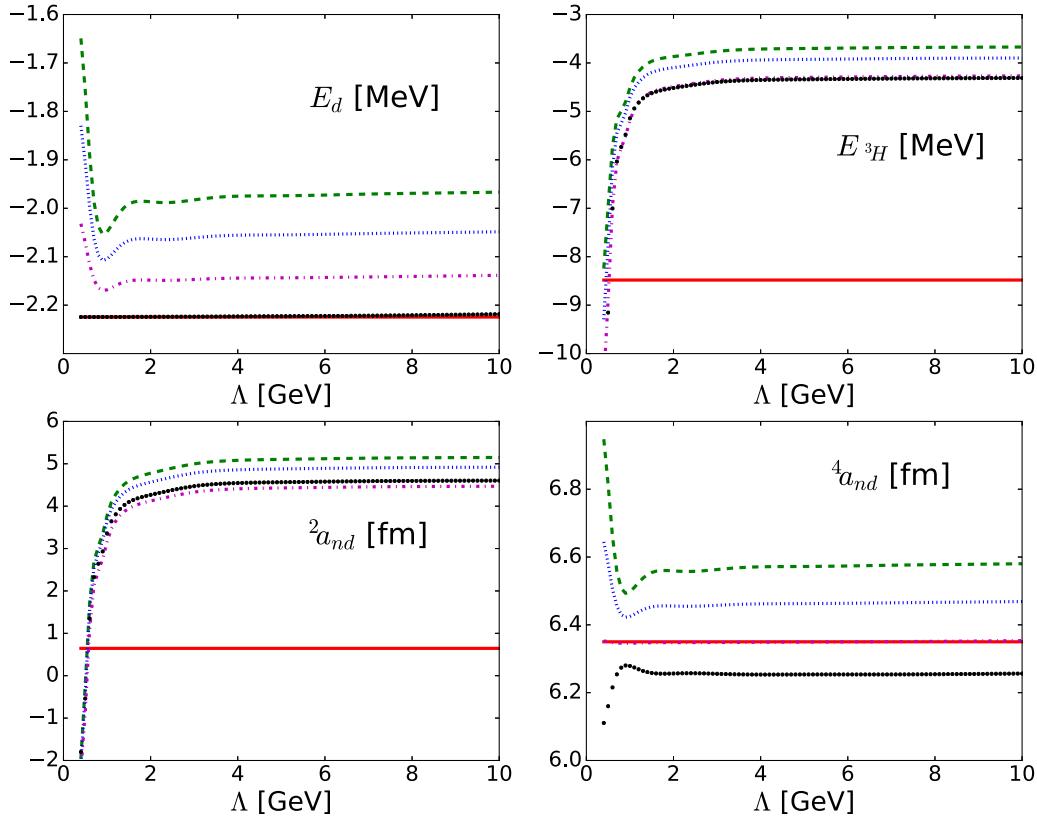

FIG. 17. Cutoff dependence of the deuteron (top left) and triton (top right) energies, and $J = 1/2$ (bottom left) and $J = 3/2$ (bottom right) neutron-deuteron scattering lengths at LO with the $n = 4$ regulator, for different fitting procedures for the two-nucleon S-wave counterterms. Results are shown for strategies (I) (green dashed line), (II) (blue dotted line), (III) (magenta dot-dashed line), and (IV) (black dots), in comparison with experiment (red solid line).

power counting where three-body forces appear at higher order. We attempt to infer the order of the short-range three-nucleon force from the residual cutoff dependence of three-nucleon observables most sensitive to this force: Those in the doublet channel, where the exclusion principle does not forbid the three nucleons to be close together. To be definite, we consider the results for the $n = 4$ regulator in the range $\Lambda \geqslant 1.2$ GeV, with counterterms fitted to the $T_L = 5$ MeV PWA93 data. From RGI, we expect inverse powers of the cutoff at large cutoff values, so we fit the triton energy with a power

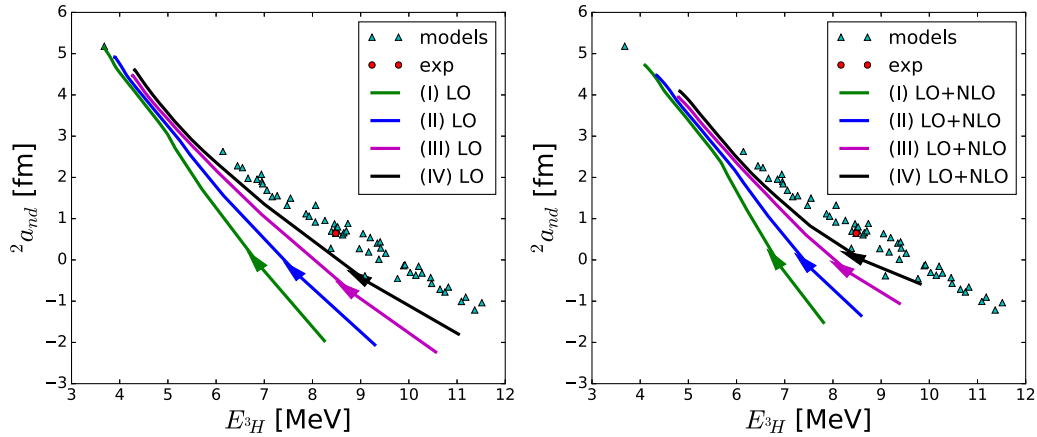

FIG. 18. Correlation between triton binding energy and *nd* doublet scattering length at leading order (left) and next-to-leading order (right). Different lines correspond to cutoff variation from the various fitting strategies, the arrow indicating the direction of increasing cutoff. Phenomenological model results (triangles) and the empirical value (circle) are also shown.

TABLE III. Parameters of fits using Eqs. (20) and (23) to the leading-order and next-to-leading-order results for the triton binding energy from fitting procedure (II) for cutoff values $\Lambda \geqslant 1.2$ GeV. The parameters $E_{^3H}^{(m)}(\infty)$ and $p_{t1,2,3}^{(m)}$ $(m = 0,1)$ are in MeV. Numbers in parentheses represent fitting errors.

LO				NLO			
$E_{^3H}^{(0)}(\infty)$	$p_{t1}^{(0)}$	$p_{t2}^{(0)}$	$p_{t3}^{(0)}$	$E_{^3H}^{(1)}(\infty)$	$p_{t1}^{(1)}$	$p_{t2}^{(1)}$	$p_{t3}^{(1)}$
−3.82	146(3)			−4.24	221(2)		
−3.88	35.8(4.6)	377(75)		−4.27	167(5)	262(80)	
−3.88	30(14)	399(194)	243(310)	−4.26	171(16)	239(208)	208(325)

series

$$E_{^3\mathrm{H}}^{(0)}(\Lambda) = E_{^3\mathrm{H}}^{(0)}(\infty)\left[1 + \frac{p_{t1}^{(0)}}{\Lambda} + \left(\frac{p_{t2}^{(0)}}{\Lambda}\right)^2 + \left(\frac{p_{t3}^{(0)}}{\Lambda}\right)^3 + \cdots\right], \tag{20}$$

with parameters $E_{^3\mathrm{H}}^{(0)}(\infty)$ and $p_{t1,2,3}^{(0)}$. Likewise, the doublet scattering length is fitted by

$${}^2a_{\mathrm{nd}}^{(0)}(\Lambda) = {}^2a_{\mathrm{nd}}^{(0)}(\infty)\left[1 - \frac{p_{d1}^{(0)}}{\Lambda} + \left(\frac{p_{d2}^{(0)}}{\Lambda}\right)^2 + \left(\frac{p_{d3}^{(0)}}{\Lambda}\right)^3 + \cdots\right], \tag{21}$$

with parameters ${}^2a_{\mathrm{nd}}^{(0)}(\infty)$ and $p_{d1,2,3}^{(0)}$. The fitting parameters are summarized in Tables III and IV, and the corresponding fits are shown in the left panels of Figs. 19 and 20. Numbers, particularly at the highest power of a truncation and in the four-parameter fit, depend somewhat on the cutoff range, regulator function, and fitting procedure. However, qualitative conclusions do not change. After they stabilize, the momenta $p_{t1}^{(0)} \sim p_{d1}^{(0)} \sim p_{s1}^{(0)}$, which is consistent with the existence of NLO corrections in the ${}^1S_0$ channel. The four-parameter fits are afflicted by large errors in the higher parameters $p_{t2,3}^{(0)}$ and $p_{d2,3}^{(0)}$, probably due to the oscillations—a consequence is the weird low-cutoff behavior of the four-parameter fit of the doublet scattering length. The large errors of this fit suggest that, again, higher-power fits would be unreliable. For the three-parameter fit, the momenta $p_{t2}^{(0)} \sim p_{d2}^{(0)}$ are somewhat large, possibly indicating larger N^{2}LO corrections.

In summary, the weak cutoff dependence of three-body observables suggests that there is no need for a three-body counterterm at LO in the RGI scheme of Nogga *et al.* [15]. This result is consistent with Weinberg's original power counting. However, considering the importance of NLO in the ${}^1S_0$ two-nucleon partial wave, we are led to consider the corresponding effects in the three-nucleon system. We first return to the two-nucleon system to quantify the NLO improvements there.

C. Two-nucleon system at NLO

As discussed earlier, an NLO correction in the ${}^1S_0$ channel is included to comply with RGI. Also, as seen in LO results, the deviation of the ${}^1S_0$ phase shift from PWA93 data appears already at low energies and cannot be cured without the NLO correction.

For the determination of NLO counterterms, we compute the NLO phase shift from a DWBA calculation with the NLO potential. We fit the counterterms to reproduce phase shifts or effective-range parameters, according to the three cases (I)–(III) listed in Table I. As an example, Fig. 21 shows the cutoff dependence of the counterterms $\tilde{C}_{^1S_0}^{(1)}$ and $\tilde{D}_{^1S_0}^{(1)}$ for fitting strategy (II). Similar dependence is found for other strategies.

In Fig. 22, we display both cutoff and energy dependence of the NLO ${}^1S_0$ phase shifts for fitting procedure (II). We have also obtained similar curves for fitting procedures (I) and (III). In comparison with Fig. 12, NLO results show decreased sensitivity to the fitting method, as desired in an EFT. The low-energy phase shifts are now found to be in good agreement with each other, and they show much improved agreement with PWA93 data, although there still remain deviations at larger energies. Our result is similar to that of Long and Yang [30], who used $T_L = 5$ and 25 MeV for fitting the counterterms. According to Ref. [30], a good reproduction of PWA93 is achieved up to $T_L \simeq 100$ MeV, once N^{2}LO ($\mathcal{O}(Q^2/M_{\mathrm{hi}}^2)$) corrections are included.

As for LO, we fit the NLO ${}^1S_0$ scattering length results from the data-fitting procedure (II) at $\Lambda \geqslant 1.2$ GeV with a

TABLE IV. Parameters of fits using Eqs. (21) and (24) to the leading-order and next-to-leading-order results for the *nd* doublet scattering length from fitting procedure (II) for cutoff values $\Lambda \geqslant 1.2$ GeV. The parameters ${}^2a_{\mathrm{nd}}^{(m)}$ and $p_{d1,2,3}^{(m)}$ $(m = 0,1)$ are in fm and MeV, respectively. Numbers in parentheses represent fitting errors.

LO				NLO			
${}^2a_{\mathrm{nd}}^{(0)}(\infty)$	$p_{d1}^{(0)}$	$p_{d2}^{(0)}$	$p_{d3}^{(0)}$	${}^2a_{\mathrm{nd}}^{(1)}(\infty)$	$p_{d1}^{(1)}$	$p_{d2}^{(1)}$	$p_{d3}^{(1)}$
5.06	193(4)			4.21	341(2)		
4.96	53.0(6.6)	433(92)		4.21	343(6)	52(93)	
4.92	47.0(16.6)	693(216)	615(332)	4.18	280(19)	430(232)	531(349)

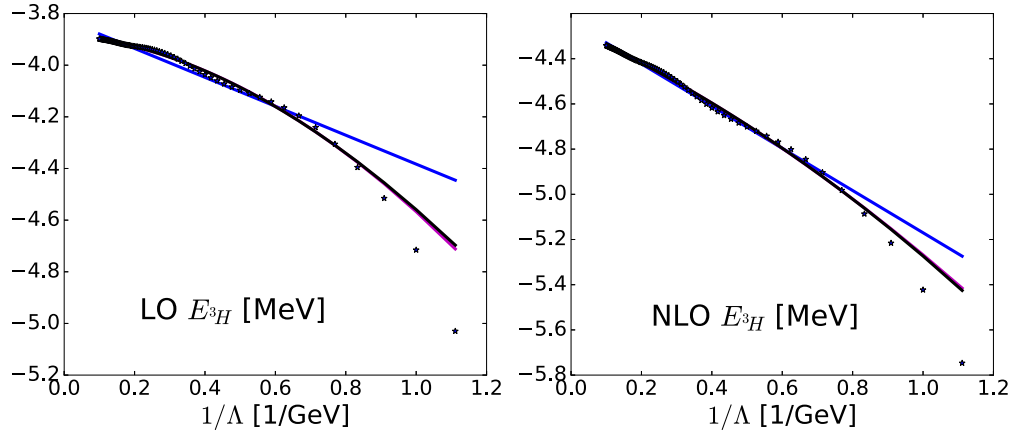

FIG. 19. Cutoff dependence of the triton binding energy at LO (left) and NLO (right) with the $n = 4$ regulator and fitting procedure (II). The blue, magenta, and black solid lines are, respectively, two-, three-, and four-parameter fits with Eqs. (20) and (23) to results for $\Lambda \geqslant 1.2$ GeV.

power series

$$a_s^{(1)}(\Lambda) = a_s^{(1)}(\infty)\left[1 + \frac{p_{s1}^{(1)}}{\Lambda} + \left(\frac{p_{s2}^{(1)}}{\Lambda}\right)^2 + \left(\frac{p_{s3}^{(1)}}{\Lambda}\right)^3 + \cdots\right]. \tag{22}$$

The fitting parameters $a_s^{(1)}(\infty)$ and $p_{s1,2,3}^{(1)}$ are also summarized in Table II and the corresponding fits are shown in the right panel of Fig. 13. The parameters are comparable to those at LO, and the asymptotic value, $a_s^{(1)}(\infty)$, is now closer to the empirical value. A better description of the low-energy data at this order can only be achieved with fitting strategy (IV). The continuing existence of Λ^{-1} dependence indicates that the next correction in this channel appears at N^{2}LO, consistent with the expectation that two-pion exchange contributes at this order [4,6,8].

In summary, NLO corrections significantly improve the description of the two-nucleon $^1S_0$ phase shift, and further improvement is expected one order higher. We now turn to the effects of the NLO potential in three-nucleon observables.

D. Three-nucleon system at NLO

With the NLO interaction so determined, we compute the NLO corrections to three-nucleon observables. Because the NLO two-nucleon interaction acts only in the $^1S_0$ channel, it does not affect the deuteron binding energy and has little effect on the nd quartet scattering length, but it is significant for the triton binding energy and the nd doublet scattering length.

Figure 23 shows the cutoff dependence of these observables at NLO. The graphs include results with the different fitting procedures listed in Table I. In all cases, cutoff independence is achieved at NLO, and the residual cutoff dependence at low cutoff values is reduced slightly.

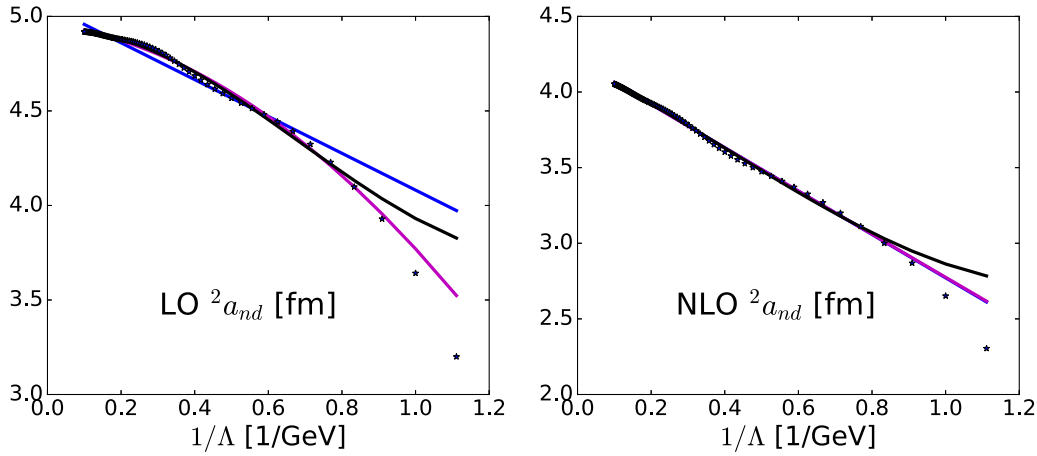

FIG. 20. Cutoff dependence of the nd doublet scattering length at LO (left) and NLO (right) with the $n = 4$ regulator and fitting procedure (II). The blue, magenta, and black solid lines are, respectively, two-, three-, and four-parameter fits with Eqs. (21) and (24) to results for $\Lambda \geqslant 1.2$ GeV.

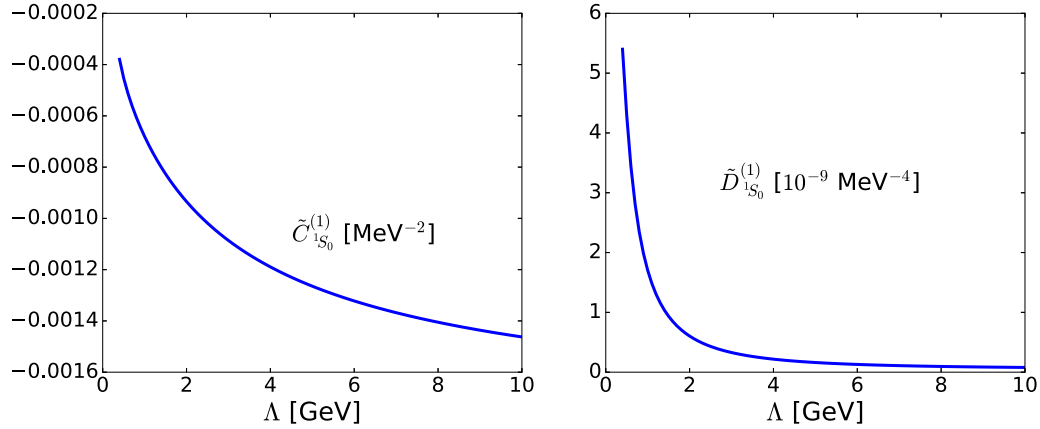

FIG. 21. Cutoff dependence of the NLO counterterms $\tilde{C}^{(1)}_{^1S_0}$ (left) and $\tilde{D}^{(1)}_{^1S_0}$ (right), with the $n = 4$ regulator. Counterterms are fitted to the PWA93 phase shifts at 5 and 10 MeV.

The right panel of Fig. 18 shows the correlation between triton binding energy and doublet scattering length at NLO, again together with model calculations. The error estimated from the cutoff dependence reduces slightly from LO to NLO. Also, the NLO result moves a bit towards the phenomenological Phillips line.

To quantify the NLO residual cutoff dependence, we perform fits analogous to Eqs. (20) and (21):

$$E^{(1)}_{^3\mathrm{H}}(\Lambda) = E^{(1)}_{^3\mathrm{H}}(\infty)\left[1 + \frac{p^{(1)}_{t1}}{\Lambda} + \left(\frac{p^{(1)}_{t2}}{\Lambda}\right)^2 + \left(\frac{p^{(1)}_{t3}}{\Lambda}\right)^3 + \cdots\right] \tag{23}$$

and

$${}^2a^{(1)}_{\mathrm{nd}}(\Lambda) = {}^2a^{(1)}_{\mathrm{nd}}(\infty)\left[1 - \frac{p^{(1)}_{d1}}{\Lambda} + \left(\frac{p^{(1)}_{d2}}{\Lambda}\right)^2 + \left(\frac{p^{(1)}_{d3}}{\Lambda}\right)^3 + \cdots\right], \tag{24}$$

with asymptotic values $E^{(1)}_{^3\mathrm{H}}(\infty)$ and ${}^2a^{(1)}_{\mathrm{nd}}(\infty)$ and parameters $p^{(1)}_{t1,2,3}$ and $p^{(1)}_{d1,2,3}$. We consider results for the $n = 4$ regulator in the range $\Lambda \geqslant 1.2$ GeV, with counterterms fitted to the PWA93 data at $T_L = 5$ MeV for LO and $T_L = 10$ MeV for NLO. The fitting parameters are again summarized in Tables III and IV, and the corresponding fits are shown in the right panels of Figs. 19 and 20.

Convergence with the cutoff implies that RGI is achieved up to NLO [$\mathcal{O}(Q/M_{\mathrm{hi}})$] without the need for a short-range three-body force. This is consistent with Weinberg's power counting. The NLO asymptotic values $E^{(1)}_{^3\mathrm{H}}(\infty)$ and ${}^2a^{(1)}_{\mathrm{nd}}(\infty)$ are closer to experiment than the LO asymptotic values $E^{(0)}_{^3\mathrm{H}}(\infty)$ and ${}^2a^{(0)}_{\mathrm{nd}}(\infty)$. Thus, NLO corrections reduce the difference between theoretical and empirical values, but they are only ~ 1 MeV for the triton binding energy and ~ 1 fm for the nd doublet scattering length. The remaining discrepancy to experiment indicates the presence of important corrections that we have not accounted for, such as N^{2}LO [$\mathcal{O}(Q^2/M^2_{\mathrm{hi}})$] corrections or perhaps lower-order interactions not needed for RGI. This is consistent with the increase in the momenta $p^{(1)}_{t,d1}$

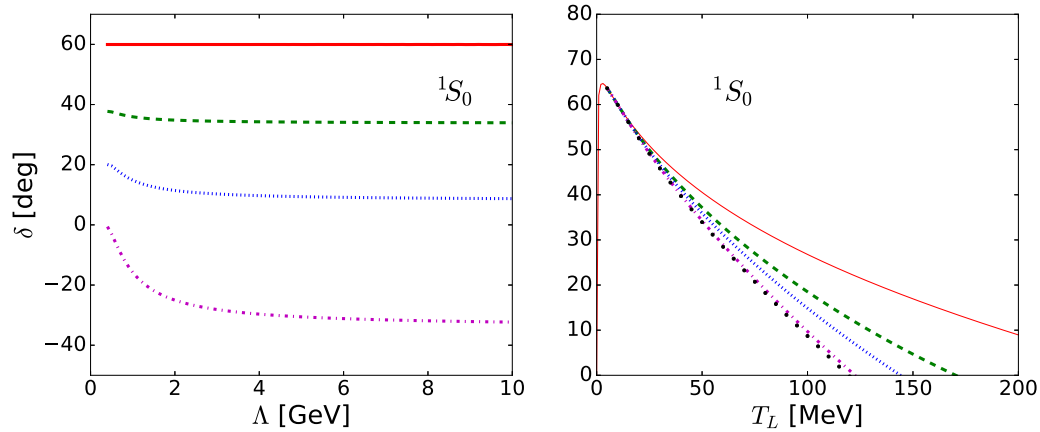

FIG. 22. NLO $^1S_0$ phase shift with the $n = 4$ regulator, for fitting method (II). Left panel: Cutoff dependence for various energies, as in Fig. 12 for LO. Right panel: Laboratory energy dependence for various cutoffs, as in Fig. 7 for LO.

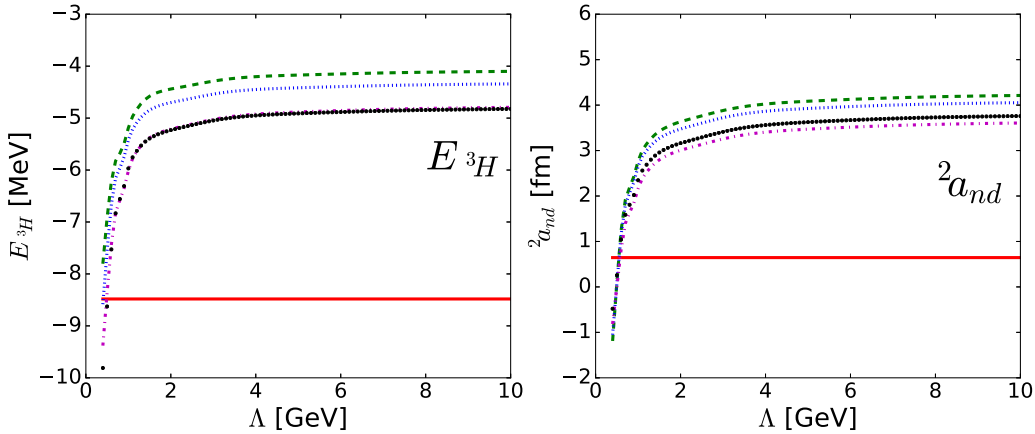

FIG. 23. Cutoff dependence of the triton energy (left) and the $J = 1/2$ neutron-deuteron scattering length (right) at NLO with the $n = 4$ regulator, for different fitting procedures for the two-nucleon S-wave counterterms. Curves as in Fig. 17.

from the LO parameters $p^{(0)}_{t,d1}$. As for LO, the four-parameter fits are plagued by large errors and probably not much can be learned from them.

IV. CONCLUSION

We have analyzed the cutoff dependence of two- and three-nucleon observables at leading and next-to-leading orders in the manifestly renormalization-group-invariant version of Chiral EFT proposed in Ref. [15] and developed in Refs. [26–30]. We have explored different regulator functions and cutoff values up to 10 GeV, as well as different fitting procedures.

At the two-nucleon level, our results agree with those in Refs. [15] and [30]. The two-nucleon interaction at LO produces results that converge as the cutoff increases and are relatively insensitive to the regulator function and fitting procedure. The residual cutoff dependence at LO indicates the need for an NLO [$\mathcal{O}(Q/M_{\rm hi})$] correction in the spin-singlet S wave. Addition of such an interaction in perturbation theory improves the description of phase shifts in this wave. We thus constructed a Chiral EFT potential up to NLO that produces a two-nucleon amplitude consistent with renormalization-group invariance.

With this potential, we have solved the Faddeev equation to calculate the triton binding energy and the two neutron-deuteron scattering lengths. At LO, the Faddeev equation is solved exactly (within numerical precision), while at NLO first-order perturbation theory is employed, as required by power counting. Our LO result for the triton binding energy again agrees with that of Ref. [15] for the same regulator function and cutoff range. In addition, we significantly expanded the cutoff range and studied the (in)sensitivity to the form of the regulator function and choice of fitting input. We also calculated the neutron-deuteron scattering lengths for the first time. We strengthen the conclusion of Ref. [15] that there is no renormalization need for a three-nucleon force at LO. We observe, again for the first time, that three-nucleon observables display similar renormalization behavior at NLO. Convergence with cutoff is achieved for different regulator functions and fitting procedures.

Results in two- and three-nucleon systems show that the modified power counting scheme of Nogga *et al.* works well with respect to renormalization, at least up to NLO. The residual cutoff dependence at NLO suggests that N^{2}LO corrections [$\mathcal{O}(Q^2/M^2_{\rm hi})$] are expected at both two- or three-nucleon levels. No conflict has been seen with the higher order of three-body forces expected on the basis of naive dimensional analysis, as prescribed in Weinberg's original power counting.

We find that the three-nucleon observables we have calculated are insensitive to two-nucleon waves with angular momentum $l \geqslant 3$. This is in agreement with numerical [15] and semianalytical [25] estimates of the importance of one-pion exchange in the two-nucleon system. Thus, our calculations are consistent with the naive expectation that the two-nucleon waves with largest phase shifts at low energies give the bulk of the contribution to few-body observables. This expectation is captured in the power counting of Nogga *et al.*, where only $l \leqslant 2$ waves are treated nonperturbatively. However, the transition in l to subleading orders is not sharp, and there is room for improvement in the treatment of various two-nucleon waves [37].

Despite the apparent self-consistency of our calculation, the triton is still considerably underbound at NLO, and the correlated doublet nd scattering length is much larger than the experimental results. It should be remembered that Friar pointed out [54] that the proper counting of factors of 4π implies that the dominant three-nucleon force in Chiral EFT with explicit Δ isobars [7] is also an NLO effect. We plan to return to this possibility in a future publication. Alternatively, the discrepancy seen here might have an origin in the relatively large distances that affect these quantities. In fact, they are very well described in Pionless EFT already at LO [35], indicating that cancelations must be present in the higher-energy Chiral EFT. Observables where cancelations occur, of course, are not ideal to test the convergence of a theory: Small corrections at higher orders can generate relatively large changes in observables from the increased imbalance between partially canceling contributions. This argument could be used as a rationale for the promotion of a higher-order three-nucleon force, as done very recently [36]. However, it is qualitatively different than the need—excluded

here—for promotion mandated by renormalization, when the very model independence of a calculation is at stake. These issues show that much of the optimal organization of Chiral EFT interactions remains to be determined, a task that requires the calculation of a larger class of observables and the inclusion of higher orders.

ACKNOWLEDGMENTS

We acknowledge useful discussions with J. Carbonell, Y. Kim, and S. König. We thank the Institute for Nuclear Theory at the University of Washington for its hospitality during the Program INT-16-1 "Nuclear Physics from Lattice QCD," when part of this work was carried out. This material is based upon work supported in part by the Rare Isotope Science Project of the Institute for Basic Science funded by Ministry of Science, ICT and Future Planning and National Research Foundation of Korea (Grant No. 2013M7A1A1075764), by the U.S. Department of Energy, Office of Science, Office of Nuclear Physics, under Award No. DE-FG02-04ER41338, and by the European Union Research and Innovation program Horizon 2020 under Grant No. 654002.

[1] S. Weinberg, Phys. Lett. B **251**, 288 (1990).
[2] M. Rho, Phys. Rev. Lett. **66**, 1275 (1991).
[3] S. Weinberg, Nucl. Phys. B **363**, 3 (1991).
[4] C. Ordóñez and U. van Kolck, Phys. Lett. B **291**, 459 (1992).
[5] S. Weinberg, Phys. Lett. B **295**, 114 (1992).
[6] C. Ordóñez, L. Ray, and U. van Kolck, Phys. Rev. Lett. **72**, 1982 (1994).
[7] U. van Kolck, Phys. Rev. C **49**, 2932 (1994).
[8] C. Ordóñez, L. Ray, and U. van Kolck, Phys. Rev. C **53**, 2086 (1996).
[9] A. Manohar and H. Georgi, Nucl. Phys. B **234**, 189 (1984).
[10] P. F. Bedaque and U. van Kolck, Annu. Rev. Nucl. Part. Sci. **52**, 339 (2002).
[11] E. Epelbaum, H.-W. Hammer, and U.-G. Meißner, Rev. Mod. Phys. **81**, 1773 (2009).
[12] R. Machleidt and D. R. Entem, Phys. Rep. **503**, 1 (2011).
[13] D. B. Kaplan, M. J. Savage, and M. B. Wise, Nucl. Phys. B **478**, 629 (1996).
[14] S. R. Beane, P. F. Bedaque, M. J. Savage, and U. van Kolck, Nucl. Phys. A **700**, 377 (2002).
[15] A. Nogga, R. G. E. Timmermans, and U. van Kolck, Phys. Rev. C **72**, 054006 (2005).
[16] M. Pavón Valderrama and E. Ruiz Arriola, Phys. Rev. C **74**, 064004 (2006); **75**, 059905(E) (2007).
[17] M. Pavón Valderrama and E. Ruiz Arriola, Phys. Rev. C **74**, 054001 (2006).
[18] D. R. Entem, E. Ruiz Arriola, M. Pavón Valderrama, and R. Machleidt, Phys. Rev. C **77**, 044006 (2008).
[19] C.-J. Yang, C. Elster, and D. R. Phillips, Phys. Rev. C **80**, 034002 (2009).
[20] C.-J. Yang, C. Elster, and D. R. Phillips, Phys. Rev. C **80**, 044002 (2009).
[21] C. Zeoli, R. Machleidt, and D. R. Entem, Few-Body Syst. **54**, 2191 (2013).
[22] D. B. Kaplan, M. J. Savage, and M. B. Wise, Phys. Lett. B **424**, 390 (1998).
[23] D. B. Kaplan, M. J. Savage, and M. B. Wise, Nucl. Phys. B **534**, 329 (1998).
[24] S. Fleming, T. Mehen, and I. W. Stewart, Nucl. Phys. A **677**, 313 (2000).
[25] M. C. Birse, Phys. Rev. C **74**, 014003 (2006).
[26] M. Pavón Valderrama, Phys. Rev. C **83**, 024003 (2011).
[27] M. Pavón Valderrama, Phys. Rev. C **84**, 064002 (2011).
[28] B. Long and C.-J. Yang, Phys. Rev. C **84**, 057001 (2011).
[29] B. Long and C.-J. Yang, Phys. Rev. C **85**, 034002 (2012).
[30] B. Long and C.-J. Yang, Phys. Rev. C **86**, 024001 (2012).
[31] M. C. Birse, Phys. Rev. C **76**, 034002 (2007).
[32] B. Long and U. van Kolck, Ann. Phys. **323**, 1304 (2008).
[33] P. F. Bedaque, H.-W. Hammer, and U. van Kolck, Phys. Rev. Lett. **82**, 463 (1999).
[34] P. F. Bedaque, H.-W. Hammer, and U. van Kolck, Nucl. Phys. A **646**, 444 (1999).
[35] P. F. Bedaque, H.-W. Hammer, and U. van Kolck, Nucl. Phys. A **676**, 357 (2000).
[36] A. Kievsky, M. Viviani, M. Gattobigio, and L. Girlanda, Phys. Rev. C **95**, 024001 (2017).
[37] M. P. Valderrama, M. S. Sánchez, C. J. Yang, B. Long, J. Carbonell, and U. van Kolck, Phys. Rev. C **95**, 054001 (2017).
[38] E. Epelbaum and U.-G. Meißner, Few-Body Syst. **54**, 2175 (2013).
[39] N. Kaiser, R. Brockmann, and W. Weise, Nucl. Phys. A **625**, 758 (1997).
[40] N. Kaiser, S. Gerstendorfer, and W. Weise, Nucl. Phys. A **637**, 395 (1998).
[41] V. G. J. Stoks, R. A. M. Klomp, M. C. M. Rentmeester, and J. J. de Swart, Phys. Rev. C **48**, 792 (1993).
[42] V. I. Kukulin and V. N. Pomerantsev, Ann. Phys. (N.Y.) **111**, 330 (1978).
[43] R. Lazauskas, Etude de la diffusion de particules lourdes sur des systèmes atomiques et nucléaires, Ph.D. thesis, Université Joseph-Fourier - Grenoble I, 2003, https://tel.archives-ouvertes.fr/tel-00004178/file/tel-00004178.pdf.
[44] R. Lazauskas and J. Carbonell, Phys. Rev. C **70**, 044002 (2004).
[45] Y.-H. Song, R. Lazauskas, and T.-S. Park, Phys. Rev. C **79**, 064002 (2009).
[46] D. R. Phillips, S. R. Beane, and T. D. Cohen, Ann. Phys. **263**, 255 (1998).
[47] E. P. Wigner, Phys. Rev. **98**, 145 (1955).
[48] U. van Kolck, Nucl. Phys. A **645**, 273 (1999).
[49] J.-W. Chen, G. Rupak, and M. J. Savage, Nucl. Phys. A **653**, 386 (1999).
[50] J. Vanasse, Phys. Rev. C **88**, 044001 (2013).
[51] B. Long, Phys. Rev. C **88**, 014002 (2013).
[52] R. Machleidt, P. Liu, D. R. Entem, and E. Ruiz Arriola, Phys. Rev. C **81**, 024001 (2010).
[53] A. C. Phillips, Nucl. Phys. A **107**, 209 (1968).
[54] J. L. Friar, Few-Body Syst. **22**, 161 (1997).